Multi-wavelength AGN spectra and modeling

Paolo Giommi
ASI

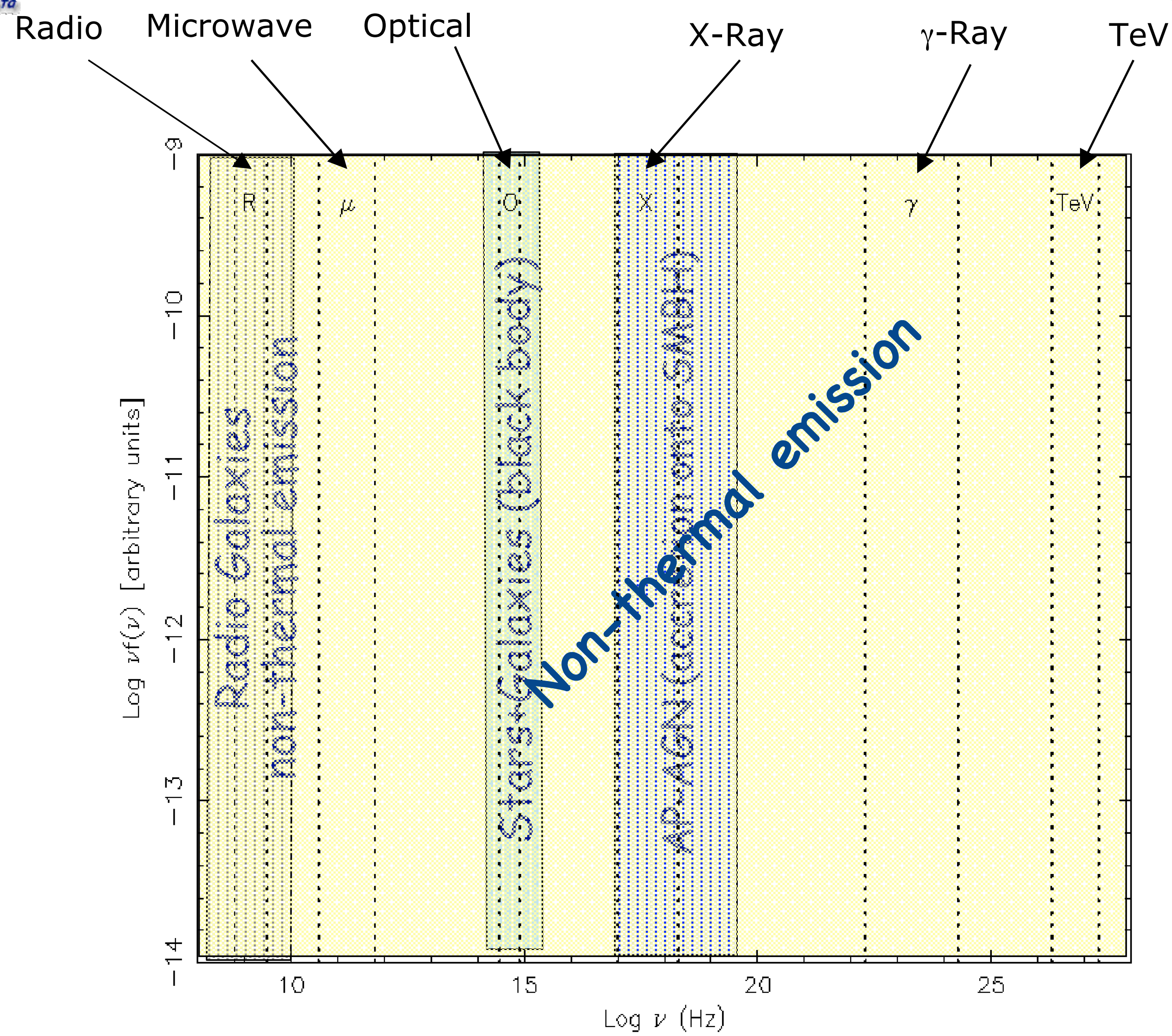

Radio
Microwave
Optical
X-Ray
γ-Ray
TeV
R
μ
O
X
γ
TeV
Radio Galaxies
non-thermal emission
Stars+Galaxies (black body)
AP-AGN (accretion onto SMBH)
Non-thermal emission
Log νf(ν) [arbitrary units]
Log ν (Hz)
−9
−10
−11
−12
−13
−14
10
15
20
25

AGN Types

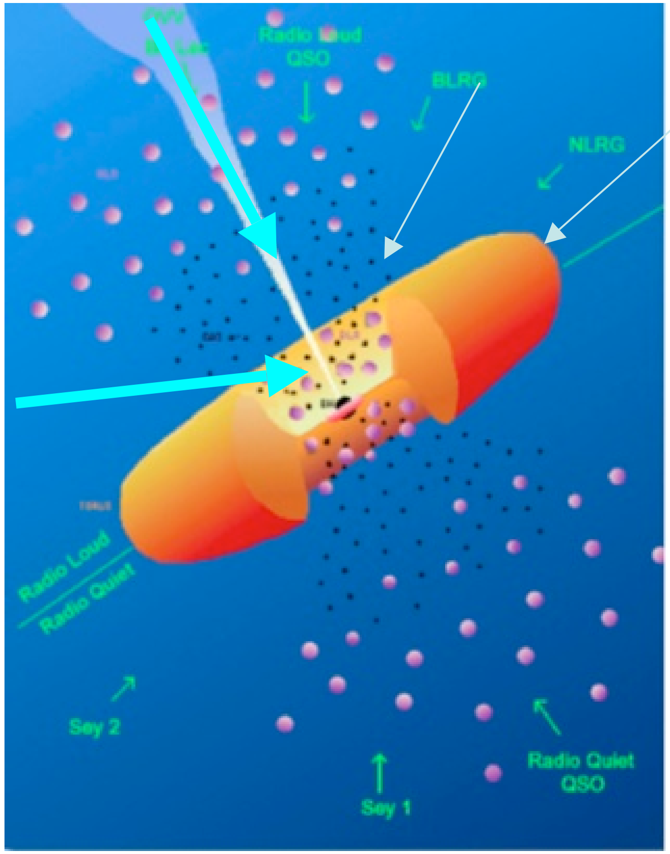

- **Accretion Dominated AGN (AD-AGN)**
  Radio-quiet QSO
  Seyfert galaxies
  Obscured AGN
  about 90% of AGN

- **Non-Thermal Radiation Dominated AGN (NT-AGN)**
  Blazars (FSRQ + BLLACS)
  Misdirected NT-AGN (Radio Galaxies, SSRQs)
  about 10% of AGN

Blazars

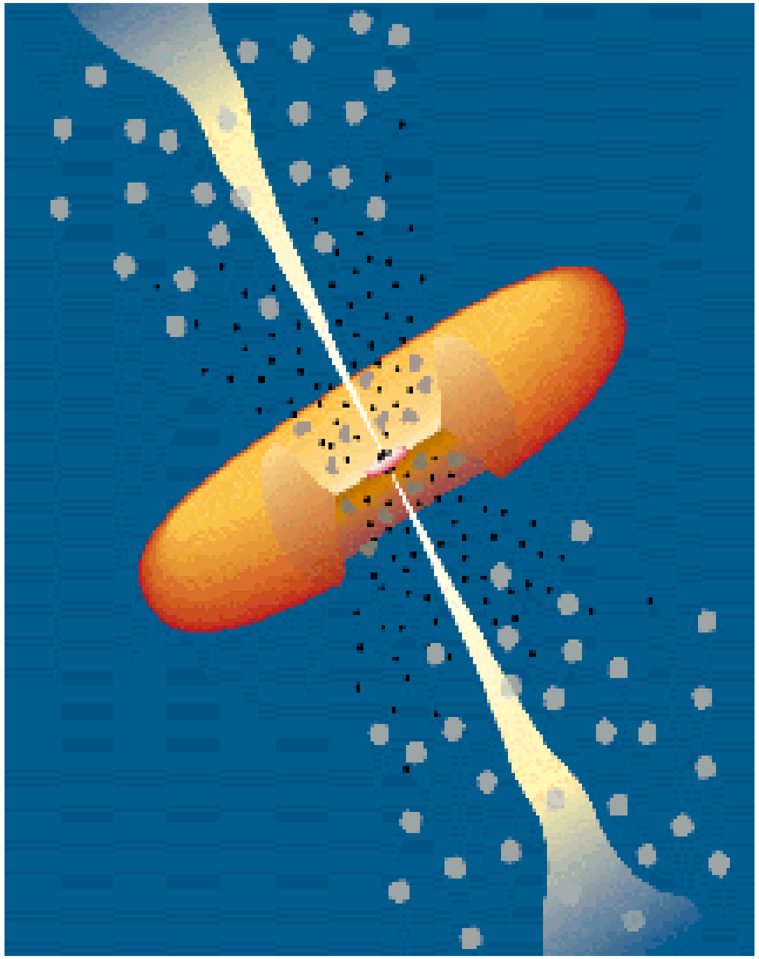

- AGN
- Highly variable at all frequencies
- Highly polarized
- Radio core dominance
- Superluminal speeds

Observed at a small angle to the jet and therefore rare AGN : 5-8% of all AGN (but only at optical or X-ray frequencies!)

Blazars are the dominant population of extragalactic point sources at

- Gamma-ray
- TeV
- Microwave frequencies

Normally the electromagnetic emission from blazars is assumed to be due to the Synchrotron-Self Compton mechanism (SSC) or SSC+External Component of a population of electrons in a jet of material that is moving at relativistic speed at a small angle with respect to the observer.

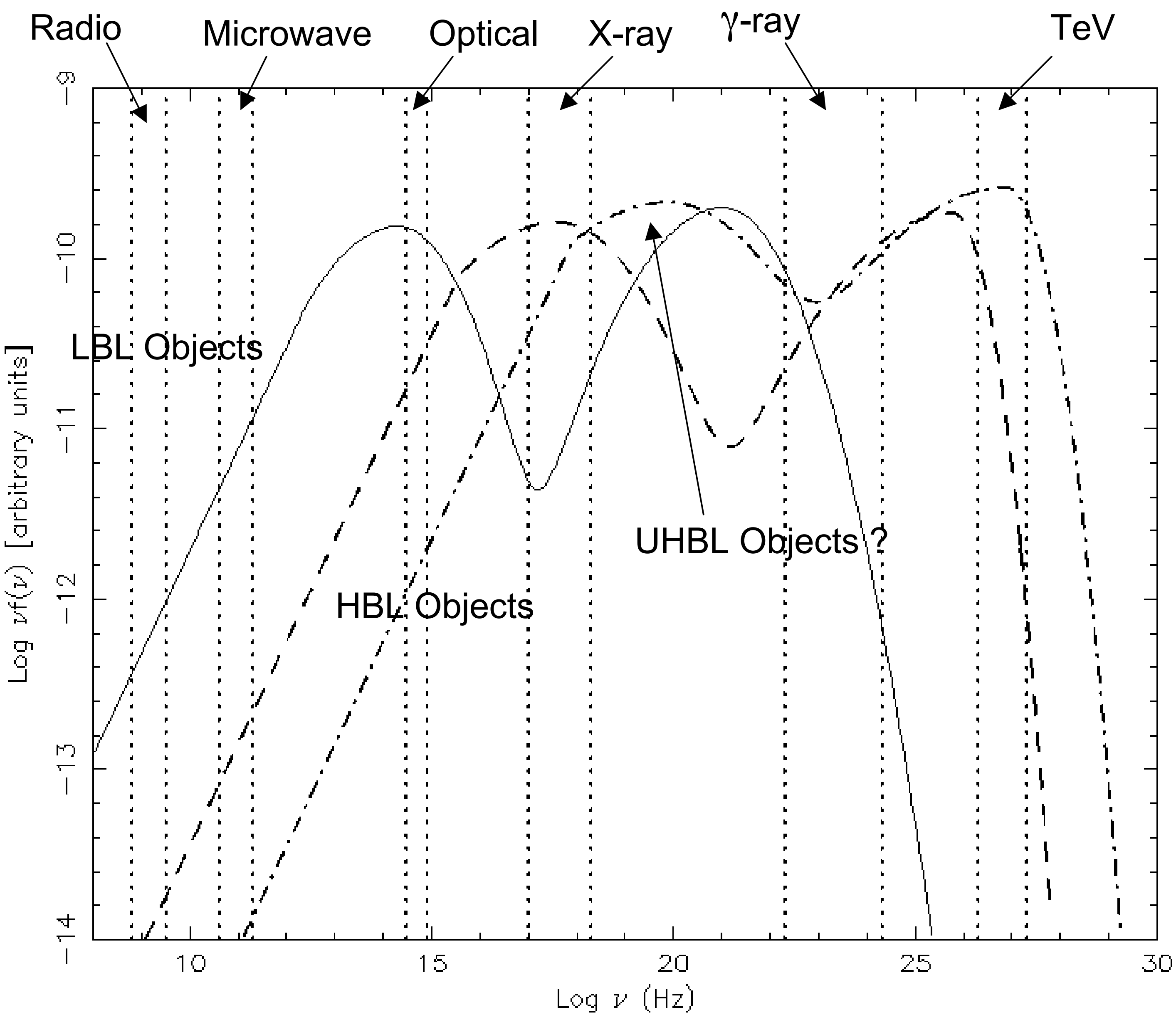

Radio
Microwave
Optical
X-ray
γ-ray
TeV
LBL Objects
HBL Objects
UHBL Objects ?
Log νf(ν) [arbitrary units]
Log ν (Hz)
-9
-10
-11
-12
-13
-14
10
15
20
25
30

Swift/AGILE ToO observations of S5 0716+714 (Oct-Nov 2007)

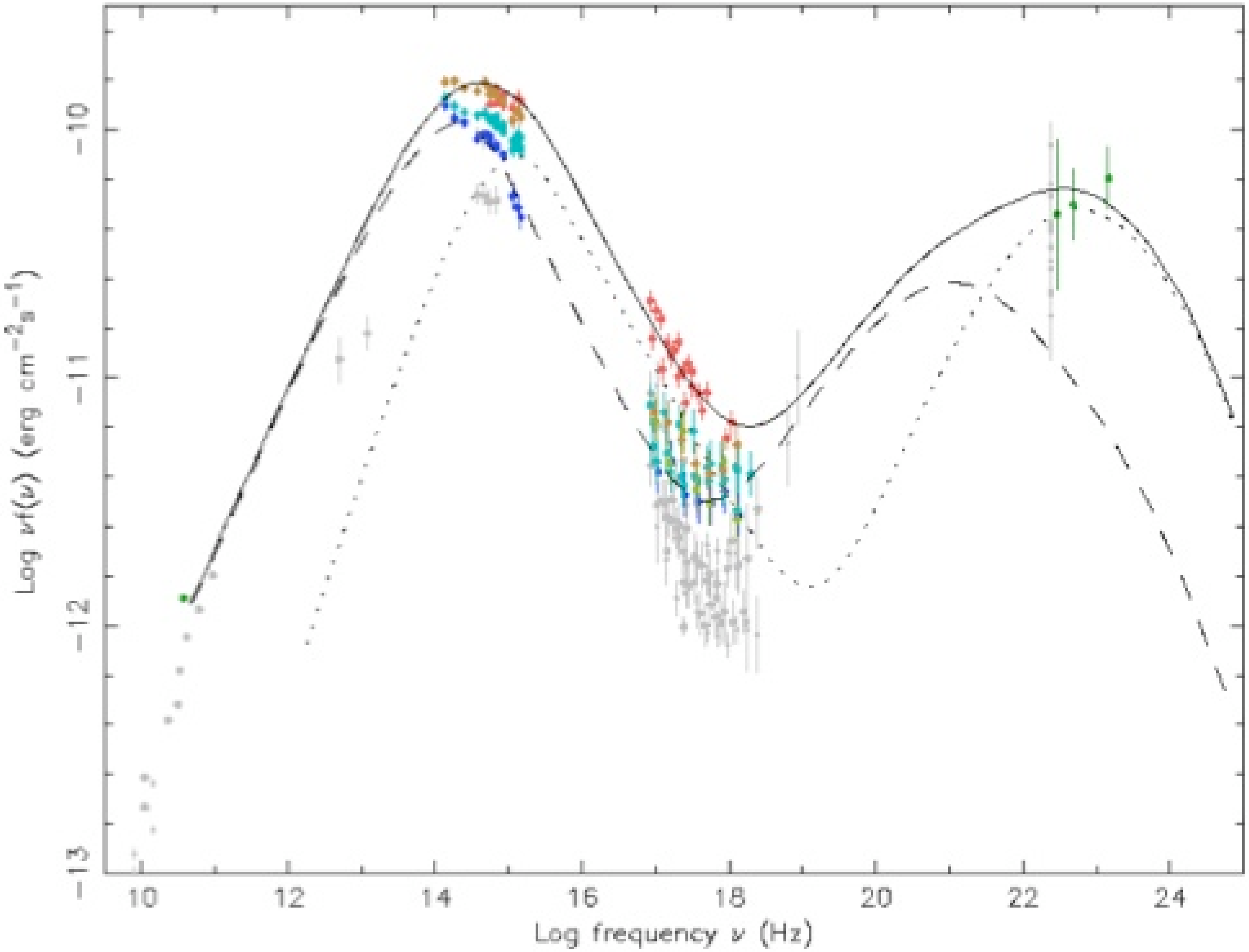

Giommi et al. 2008, A&A in press, arXiv:0806.1855

Swift observations of 3C454.3
during the giant flare of May 2005

Giommi et al. 2006, A&A 456, 911

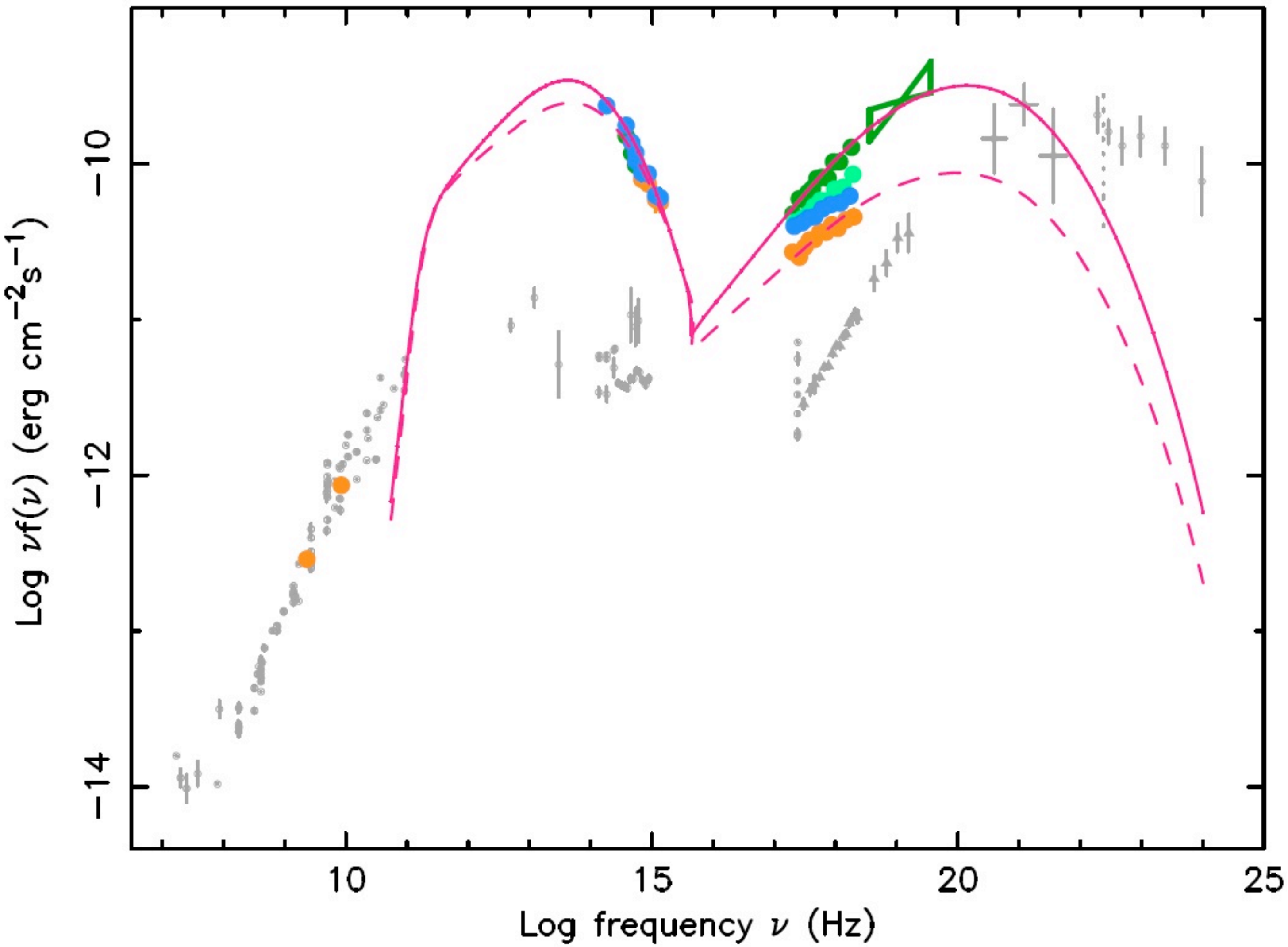

TeV dectected BL Lacs

Tramacere et al. 2006

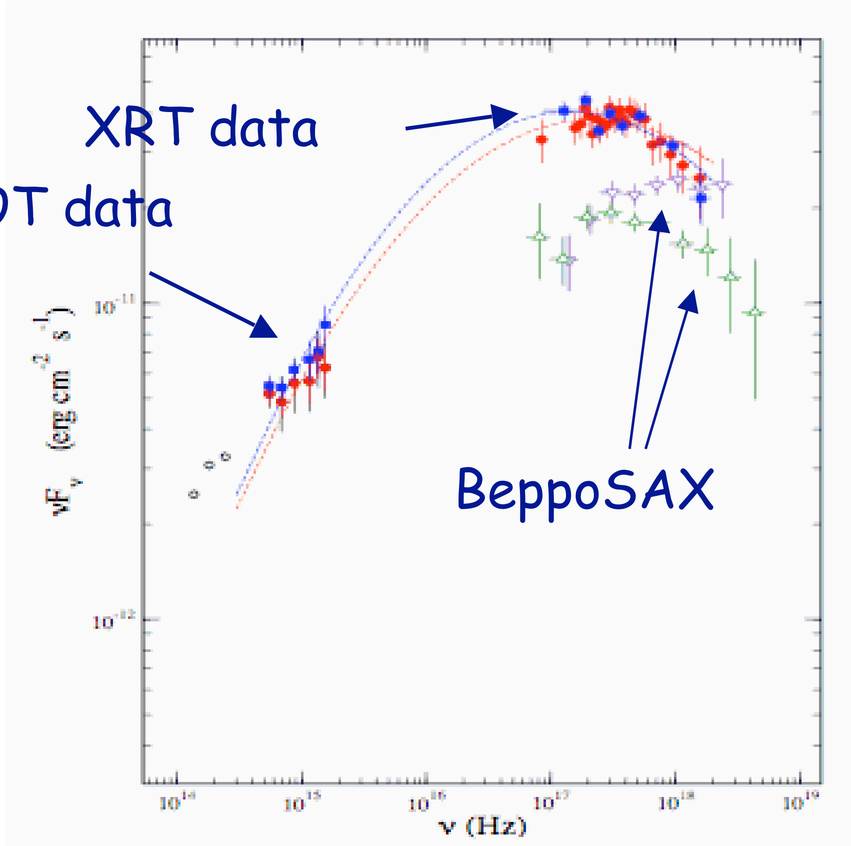

SED of 1H1100 - 230 observed on 30 June (blue) and 13 July 2005 (red). BeppoSAX 1997 and 1998 data are shown as open symbols.

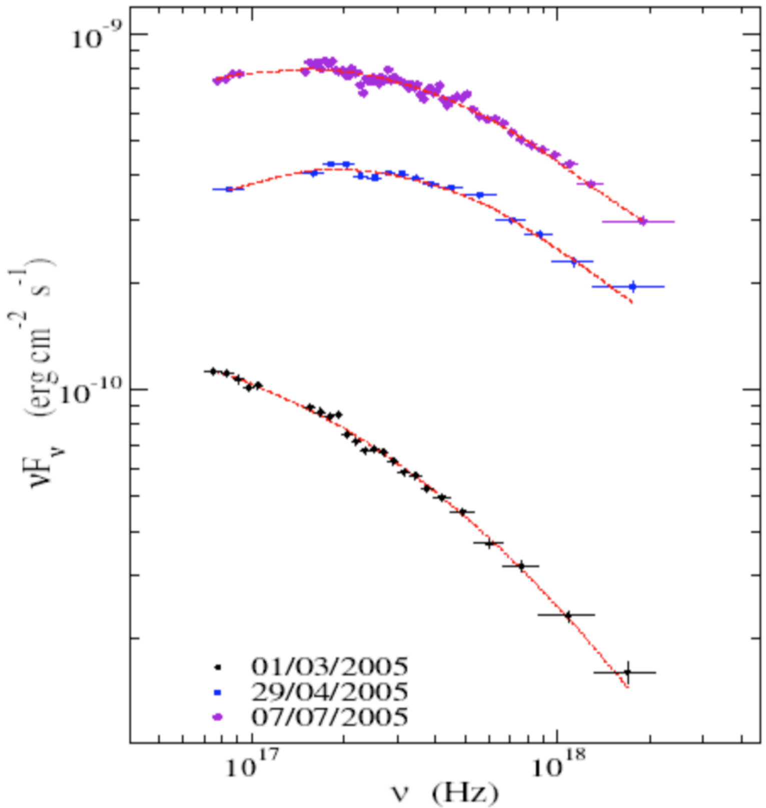

SED of MRK 421 in 2005: large changes in luminosity and peak energy.

TeV dectected BL Lacs

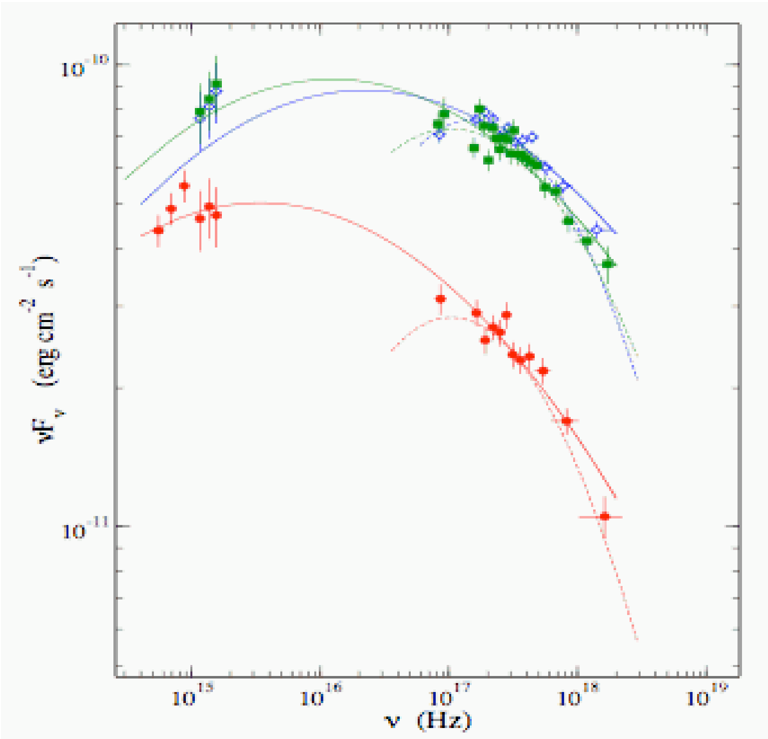

SED of 1ES 1553+113 observed on 20 April (red), 6 Octobe (blue), and 8 October 2005 (green)

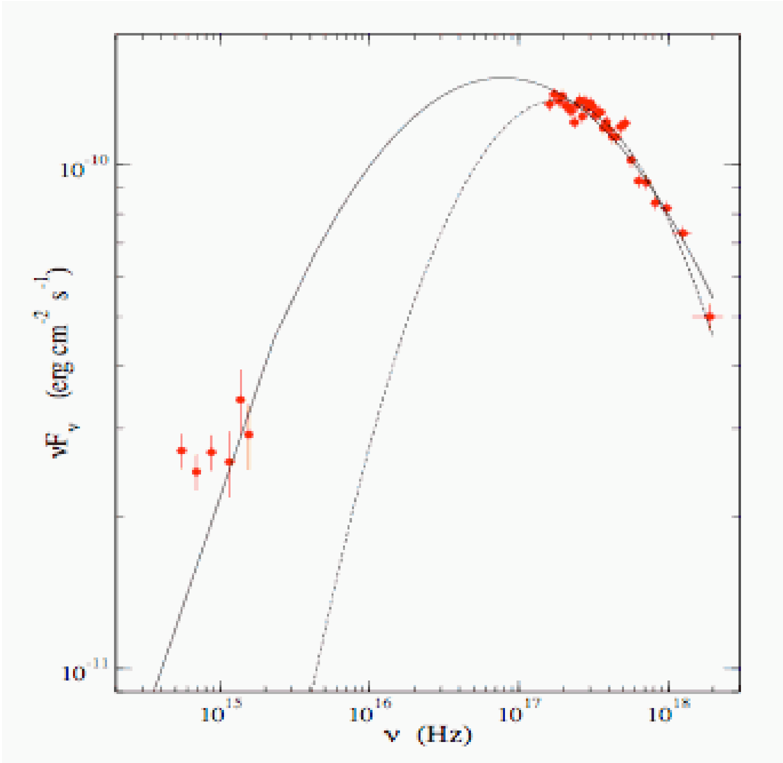

SED of 1ES 1959+650 (19 April 2005)

MKN421 in a bright state:

the BeppoSAX observation of May 2000

Massaro, Perri, Giommi, Nesci, 2004 A&A

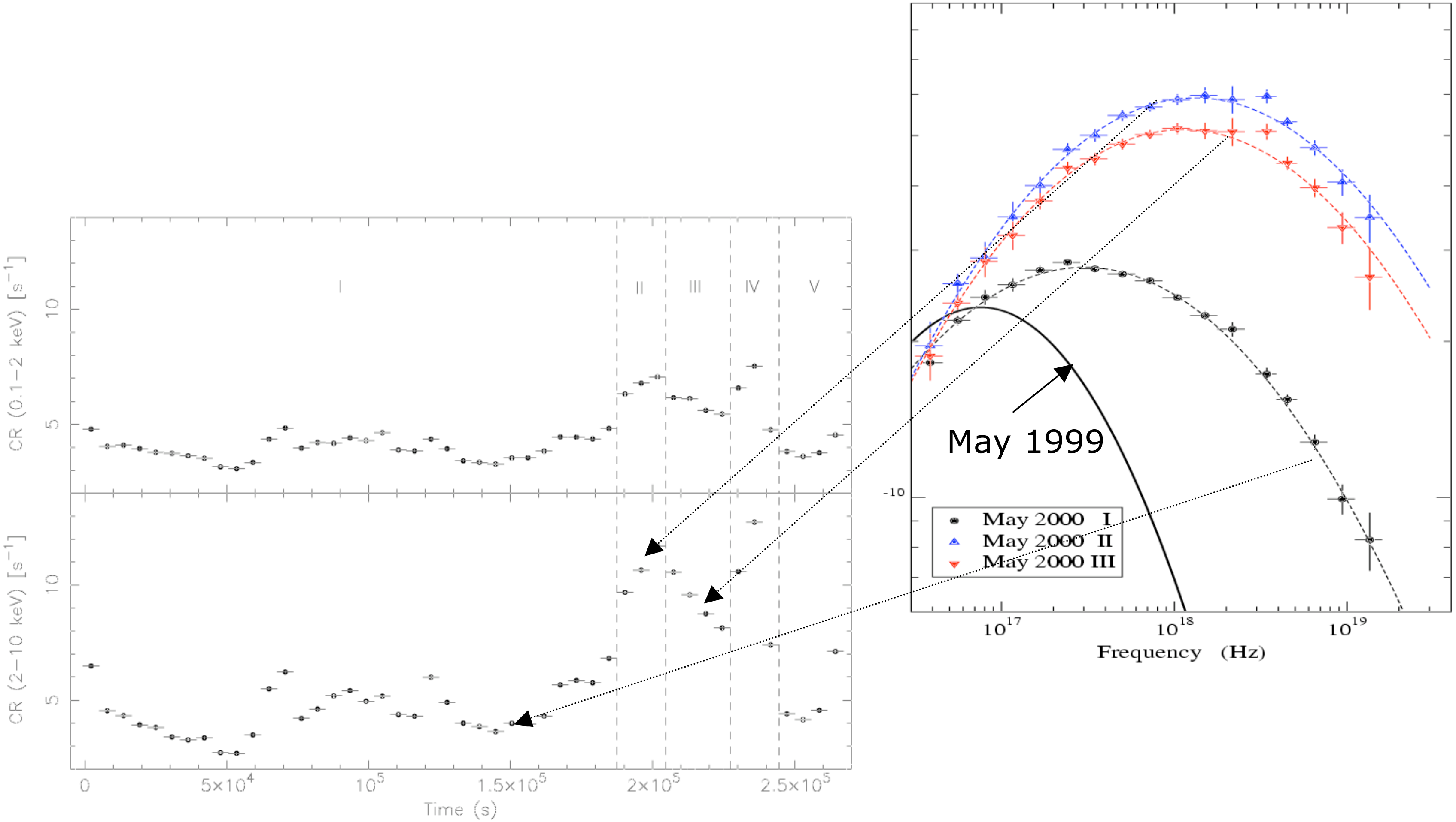

Log parabolic photon spectra can be explained as due to Synchrotron radiation from a log-parabolic particle distribution

(Massaro et al. 2004a A&A 413, 489, 2004b, A&A 422,103)

Log-parabolic spectra and particle acceleration in blazars. III: SSC emission in the TeV band from Mkn 501

E. Massaro[1], A. Tramacere[1], M. Perri[2], P. Giommi[2], and G. Tosti[3]

SSC from a log parabolic electron distribution

(Massaro et al. 2005, in press)

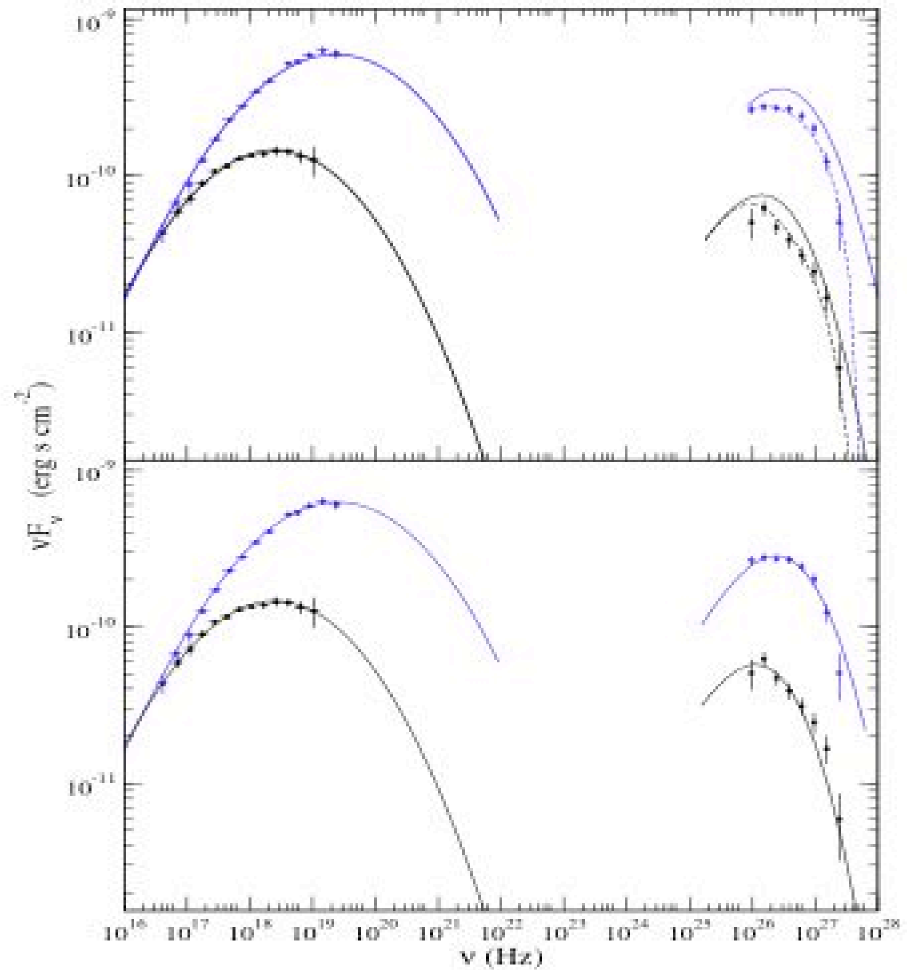

Fig. 11. Two Spectral Energy Distributions of Mkn 501 during the low and high states observed on 7 and 16 April 1997, respectively. X-ray points are from Paper II, TeV points are simultaneous CAT data (Djannati-Atai et al. 1999). Solid lines are the spectra computed in a 1-zone SSC model for the SR and IC components. In the upper panel IC spectra have been absorbed (dashed lines) by interaction with infrared EBL photons according to the LLL model by Dwek and Krennich (2005). In the lower panel EBL absorption was neglected.

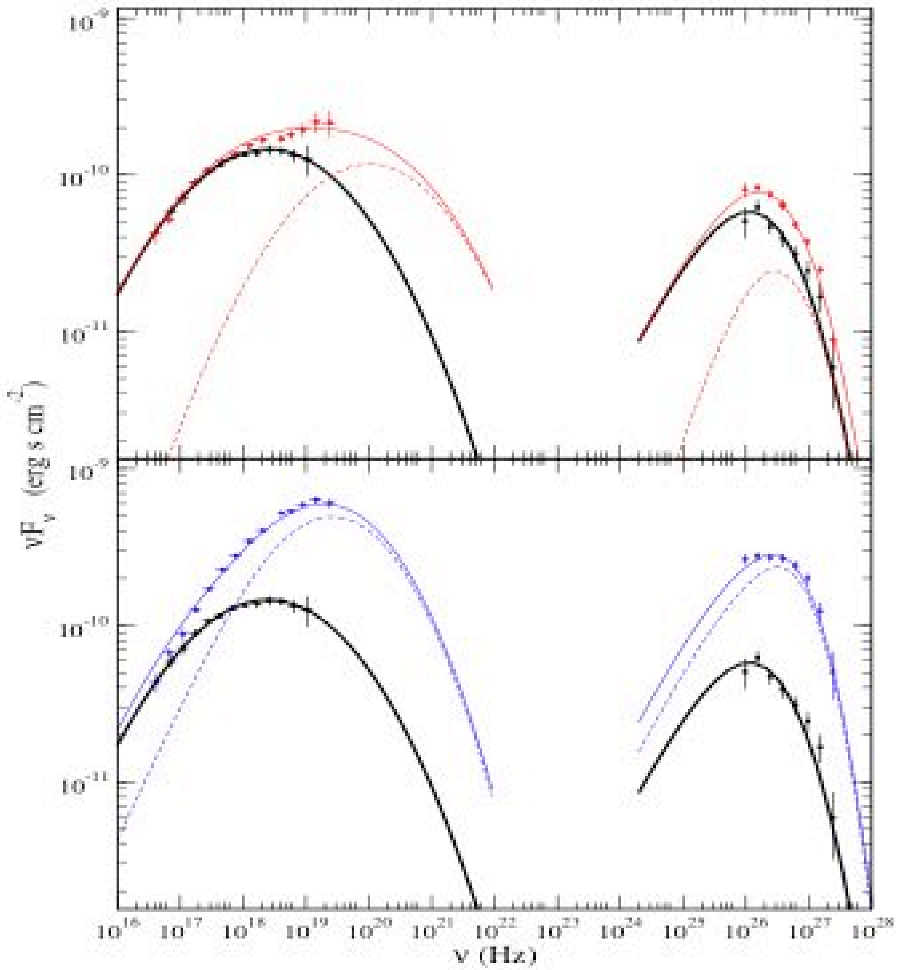

Fig. 12. Two Spectral Energy Distributions of Mkn 501 during the high states observed on 7, 11 April 1997 (upper panel) and 7, 16 April 1997 (lower panel). X-ray points are from Paper II, TeV points are simultaneous CAT data (Djannati-Atai et al. 1999). Thin solid lines are the spectra computed in a 2-zone SSC model for the SR and IC components, dashed lines are the spectra of the high-energy flaring component and thick solid line is that of slowly evolving component.

- Spectral curvature observed around the Synchrotron peak is due to intrinsic curvature of emitting particle distribution
- SSC of a particle distribution distributed as a Log-Parabola implies intrinsic curvature around Inverse Compton peak leaving little room for curvature resulting from EBL absorption
- Absorption due to EBL could be significantly lower than previously thought
- Supported also by
  - Aharonian et al. 2005 A&A 437, 395

    Cut off energy in TeV spectrum of MKN421 (3.1TeV) lower than that of MKN501 (6.2 TeV), but redshift is very similar
  - Aharonian et al. 2005 astro/ph 0508073

    HESS detection of the "high redshift" Blazars:

    H2356-309 (z=0.165) and 1ES1101-232

5. Statistical particle acceleration and log-parabolic spectra

5.1. Energy distribution of accelerated particles

The energy spectrum of accelerated particles by some statistical process, like a shock wave, is usually written as a power law

$$N(>\gamma) = No(\gamma/\gamma_0)^{-s} \quad , \tag{6}$$

where $N(>\gamma)$ is the number of particles having a Lorentz factor greater than γ and s is the spectral index given by:

$$s = -\frac{Log\ p}{Log\ \epsilon} \quad , \tag{7}$$

here p is the probability that a particle is subject to the acceleration step i in which it has an energy gain equal to ϵ assumed both independent of energy :

$$\gamma_i = \epsilon\gamma_{i-1} \tag{8}$$

and

$$N_i = pN_{i-1} = N_0\ p^i \quad . \tag{9}$$

A log-parabolic energy spectrum follows when the condition that p is independent of energy is released and one assumes that it can be described by a power relation as:

$$p_i = g/\gamma_i^q \quad , \tag{10}$$

where g and q are constant; in particular, for $q > 0$ the probability for a particle to be accelerated is lower and lower when its energy decreases. Such a situation can be realized, for instance, if particles are confined by a magnetic field with confinement efficiency decreasing for an increasing gyration radius. After simple calculations opne finds instead of Eq.(9):

$$N_i = N_0\ \frac{g^i}{\prod_{j=0}^{i-1}\gamma_j^q} \quad . \tag{11}$$

Using Eq.(8) one can write this product as:

$$\prod_{j=0}^{i-1}\gamma_j^q \;=\; \gamma_0^{iq}\prod_{j=1}^{i-1}\epsilon^{jq} \;=\; \gamma_0^{iq}\ (\epsilon^q)^{i(i-1)/2} \quad , \tag{12}$$

where γ_0 is the initial Lorentz factor of the particles; inserting this result into Eq.(11) we obtain:

$$N_i = N_0\ (\frac{g}{\gamma_0^q})^i\ (\epsilon^q)^{i(i-1)/2} \quad . \tag{13}$$

Finally, combining this equation with Eq.(8) one can obtain the integral energy distribution of the accelerated particles:

$$N(>\gamma) = N_0(\gamma/\gamma_0)^{-s+r\,Log(\gamma/\gamma_0)} \quad , \tag{14}$$

with

$$s = -\frac{Log(g/\gamma_0)}{Log\ \epsilon} - \frac{q}{2} \tag{15}$$

Swift observation of MKN421 in 2006

Tramacere et al. 2008 in preparation

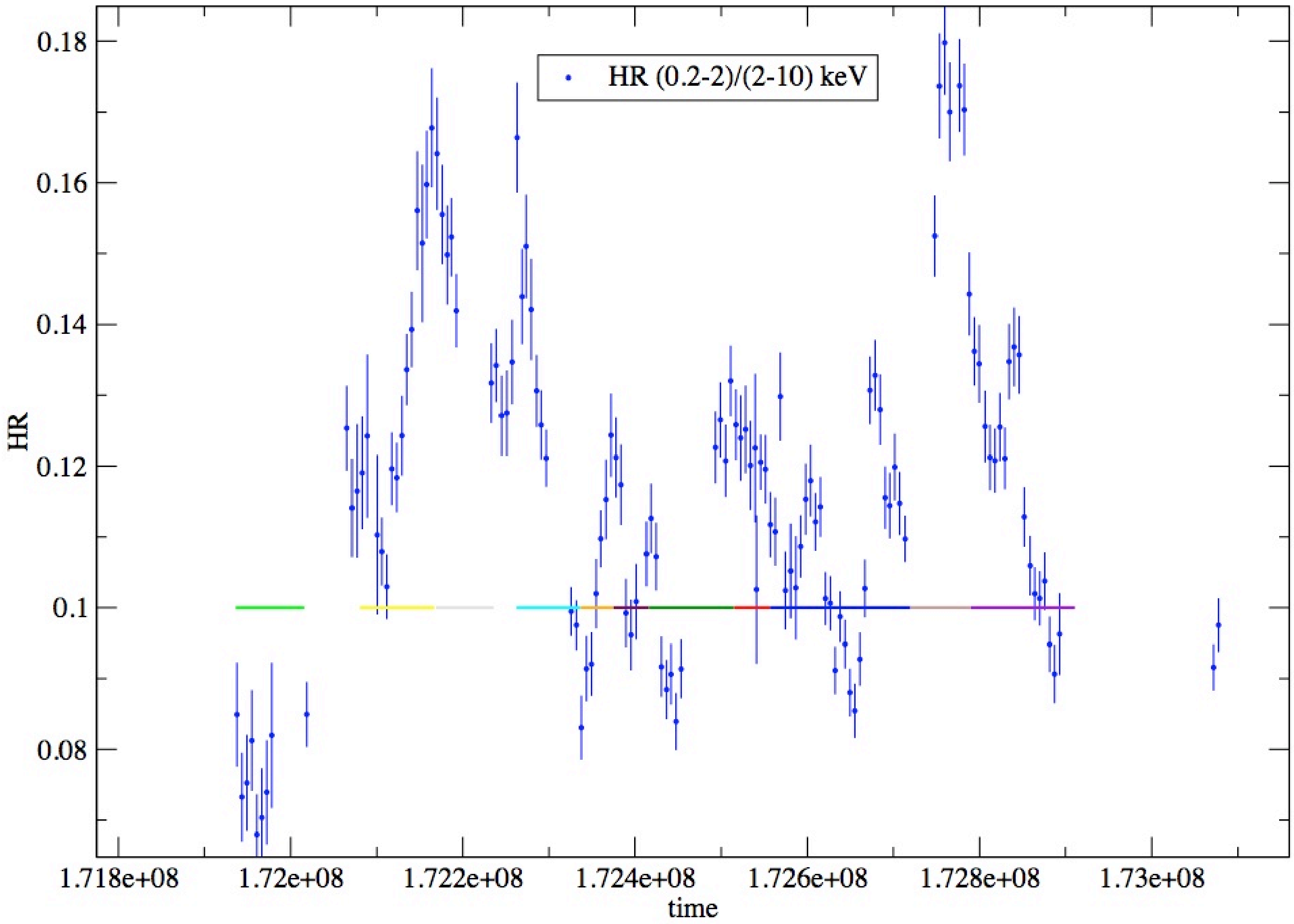

WMAP bright foreground source catalog

208 bright sources, of which

WMAP CMB fluctuation map

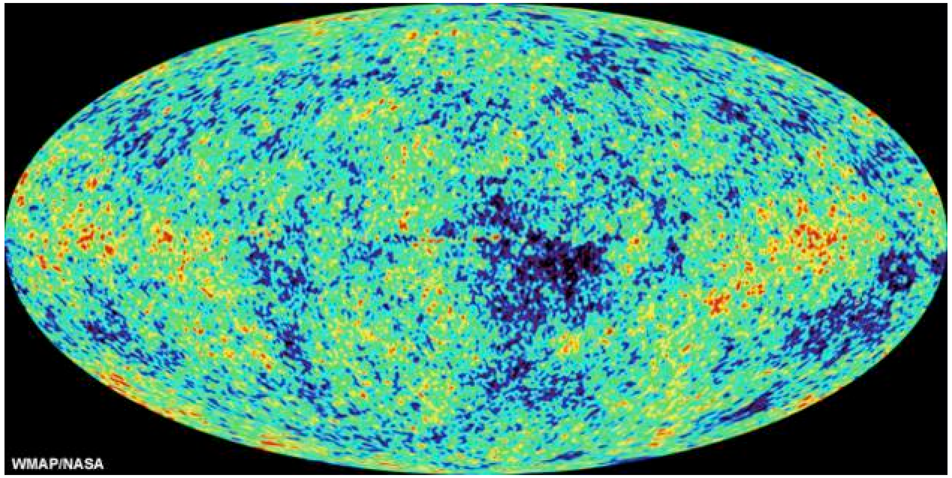

- 140 FSRQs
- 23 BL Lacs
- 13 Radio galaxies
- 5 Steep Spectrum QSOs
- 2 starburst galaxies
- 2 planetary nebule

- 17 unidentified
- 6 without radio counterpart (probably spurious)

The vast majority of bright WMAP foreground sources are Blazars

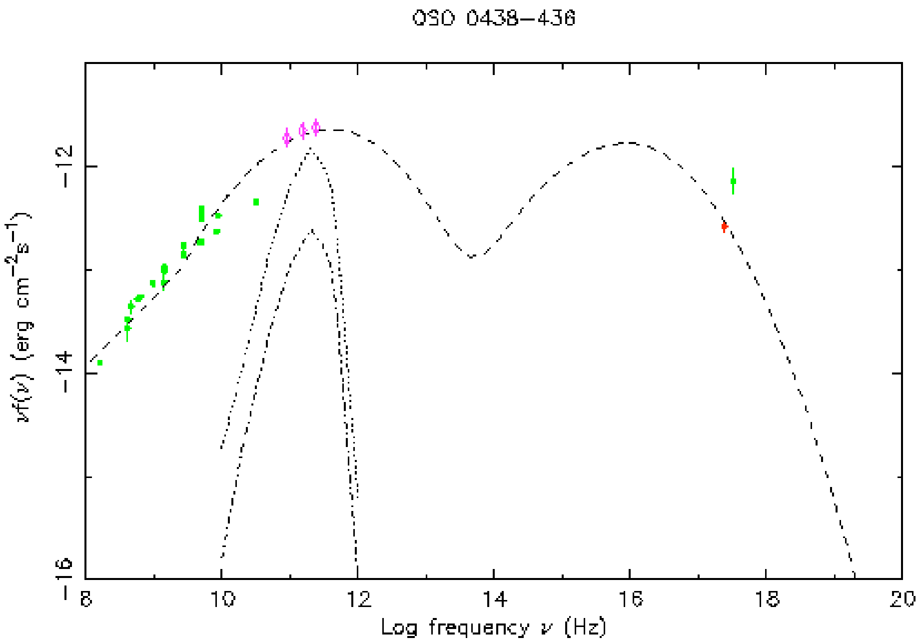
QSO 0438−436
−12
−14
−16
8
10
12
14
16
18
20
νf(ν) (erg cm^{-2}s^{-1})
Log frequency ν (Hz)

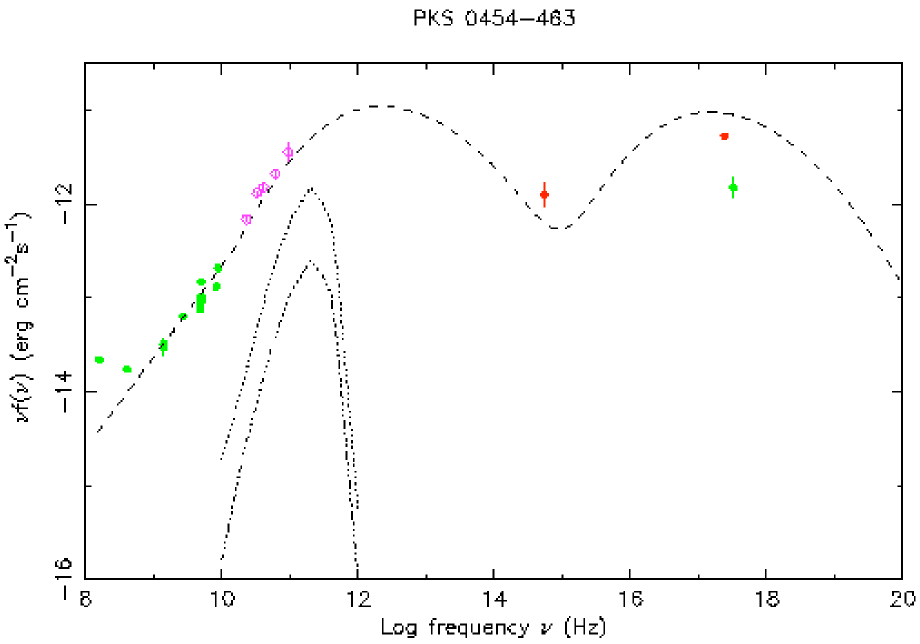
PKS 0454−463
−12
−14
−16
8
10
12
14
16
18
20
νf(ν) (erg cm^{-2}s^{-1})
Log frequency ν (Hz)

Radio Galaxy PKS 0518-45

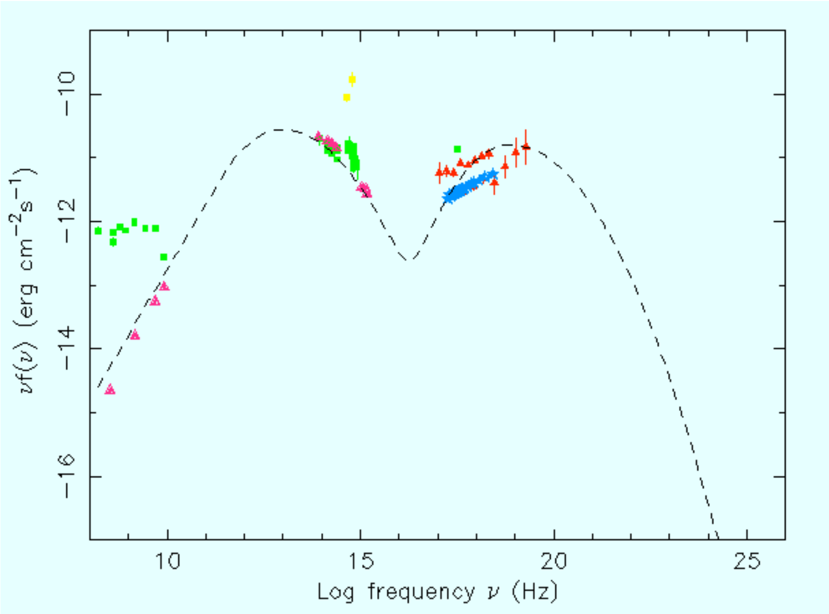

Radio Galaxy 3C 111

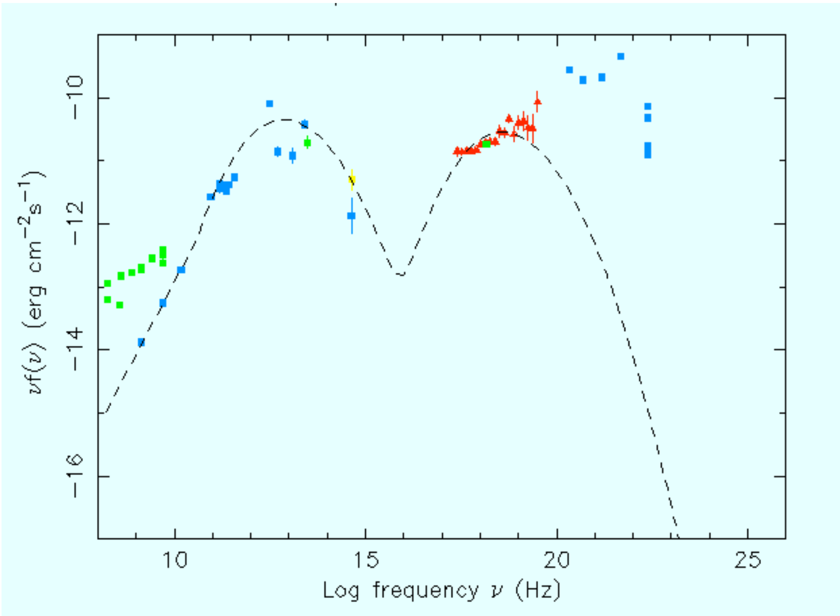

Fiocchi, Grandi et al. in preparation

Boomerang 90 GHz CMB MAP
De Bernardis et al. 2000

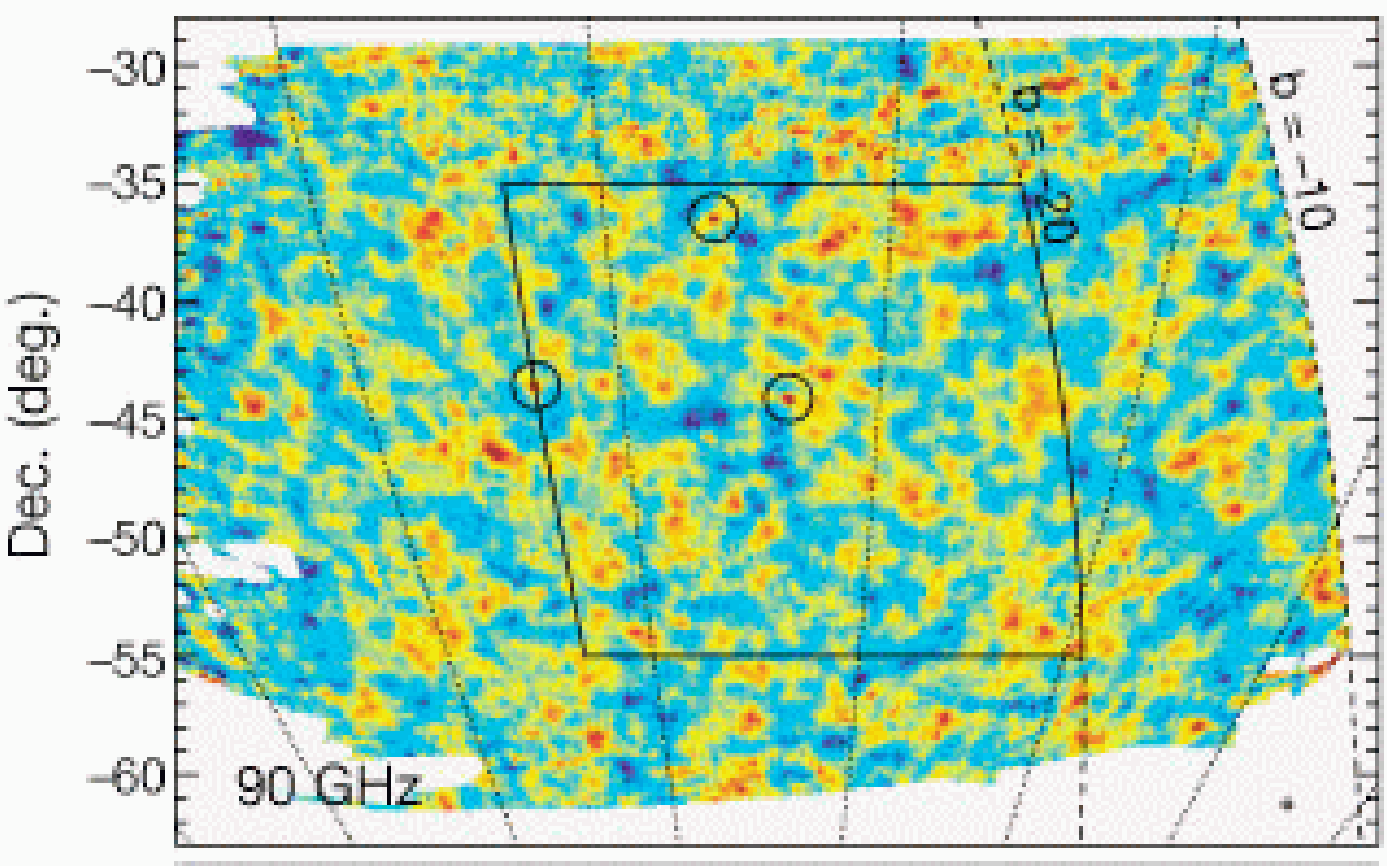

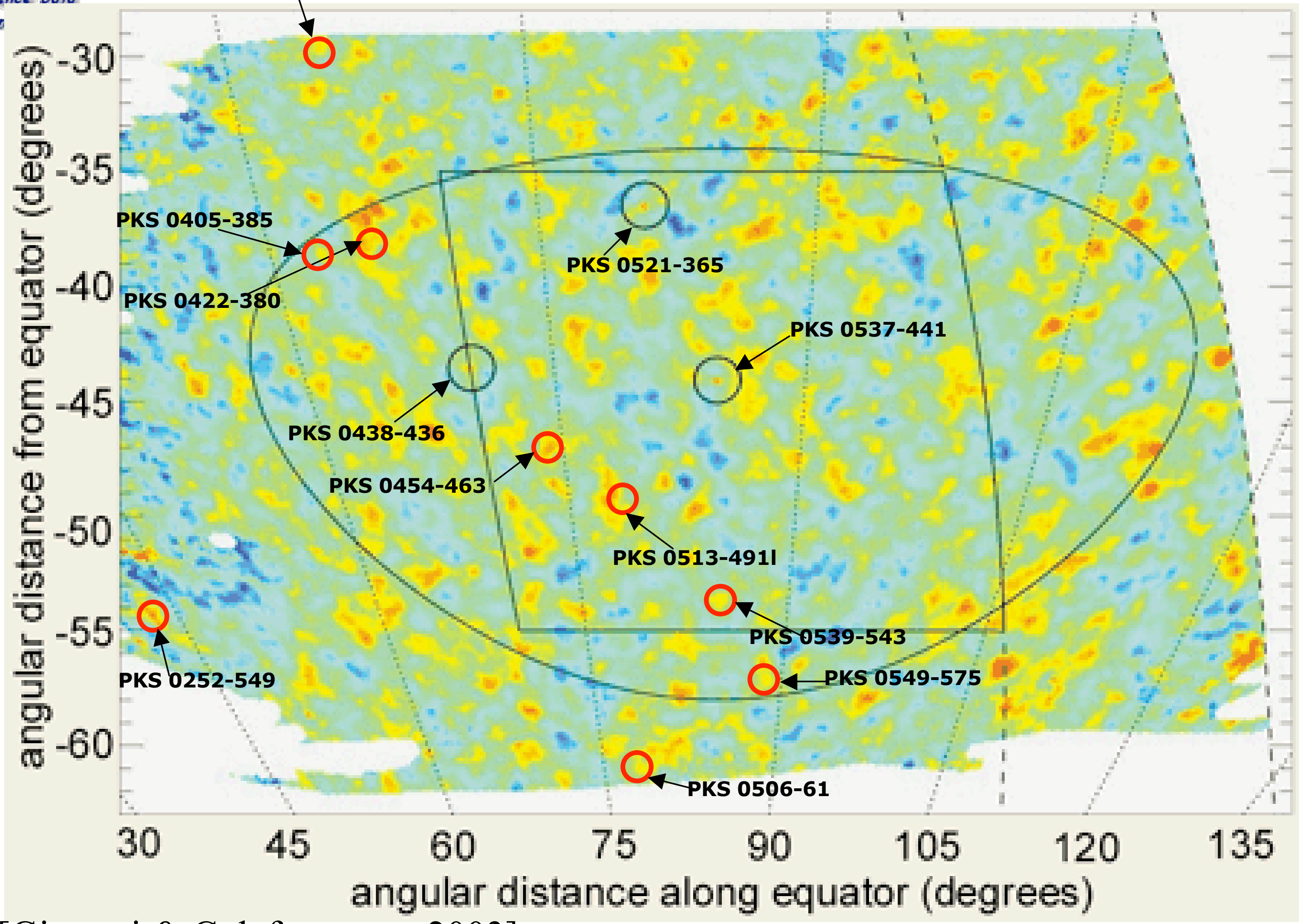

[Giommi & Colafrancesco 2003]

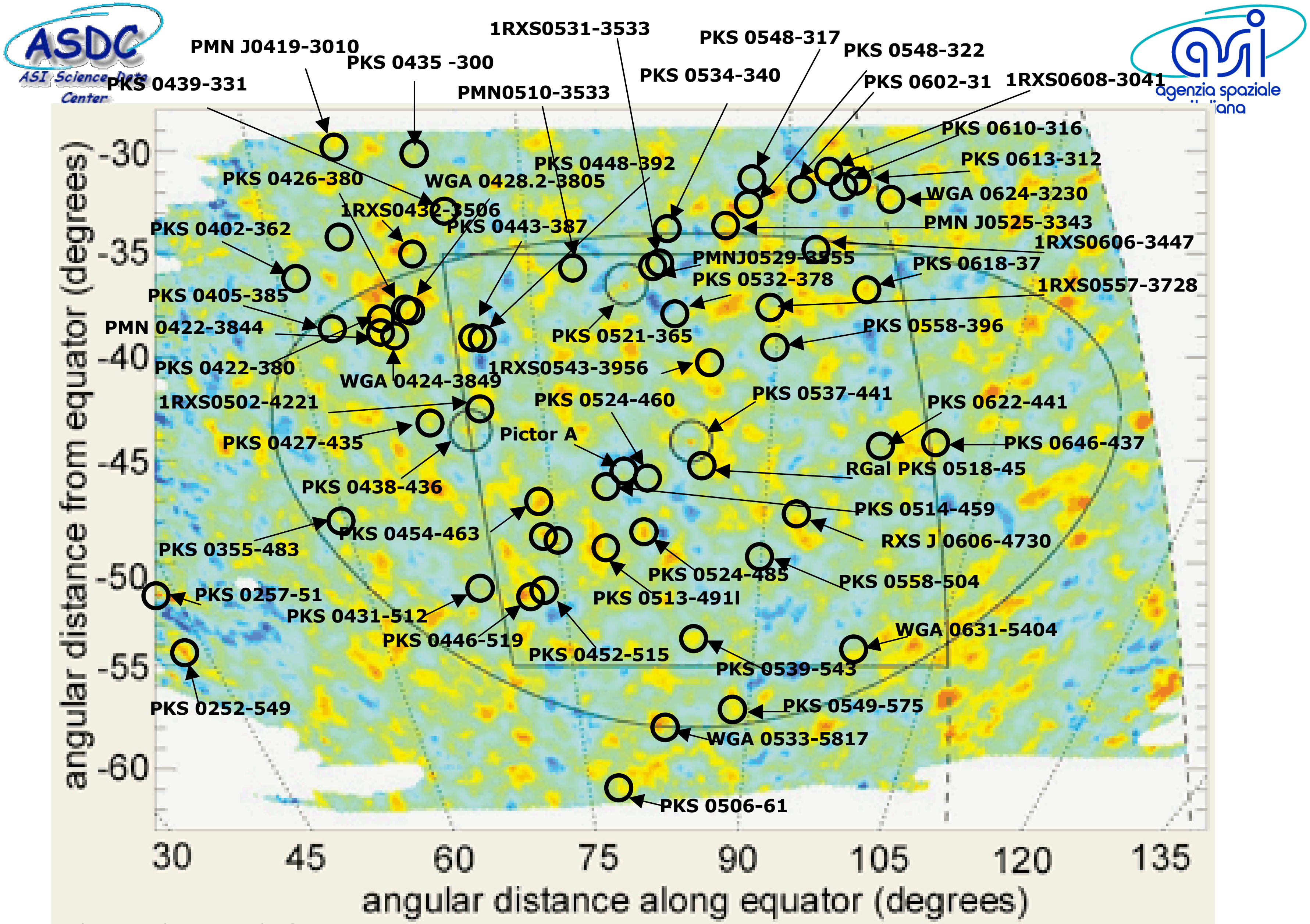

[Giommi & Colafrancesco 2003]

WMAP SEDs

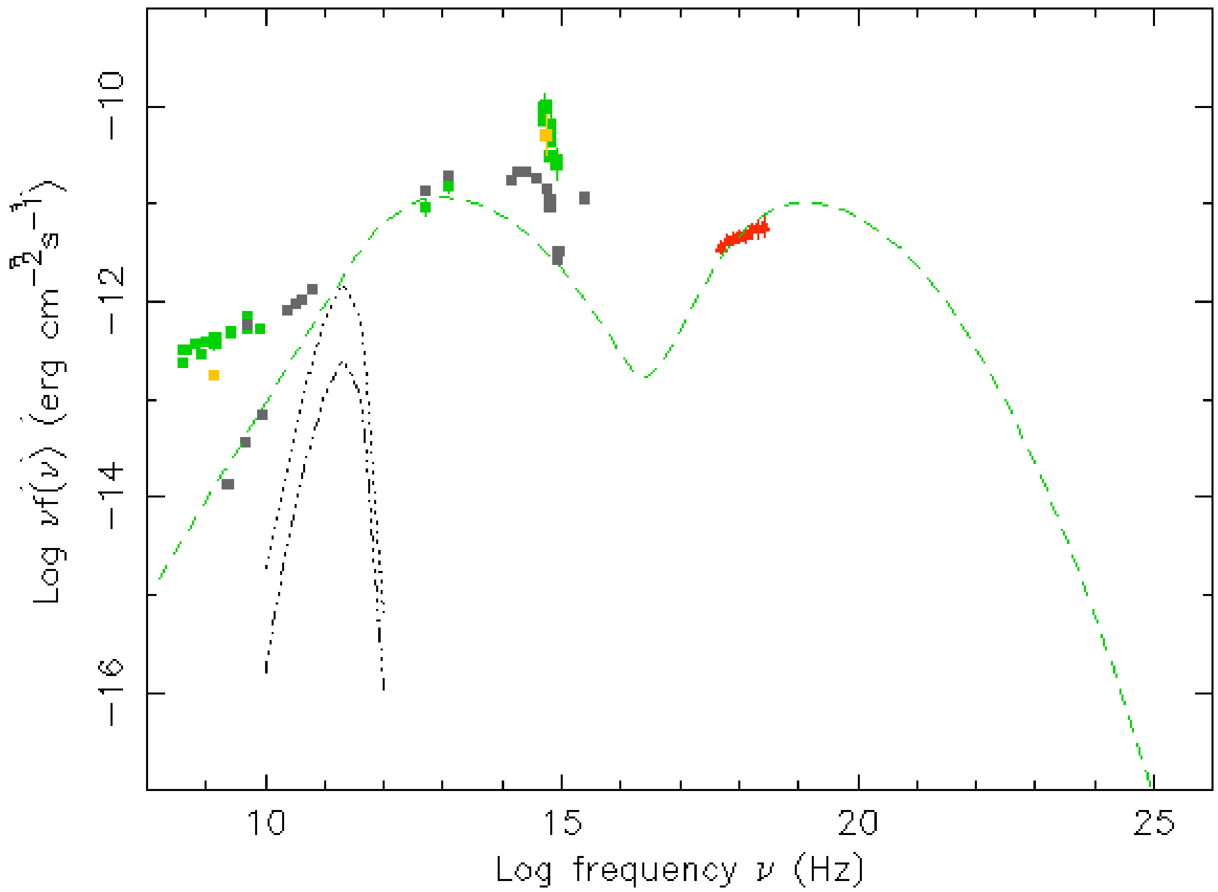

The Blazar LogN-LogS

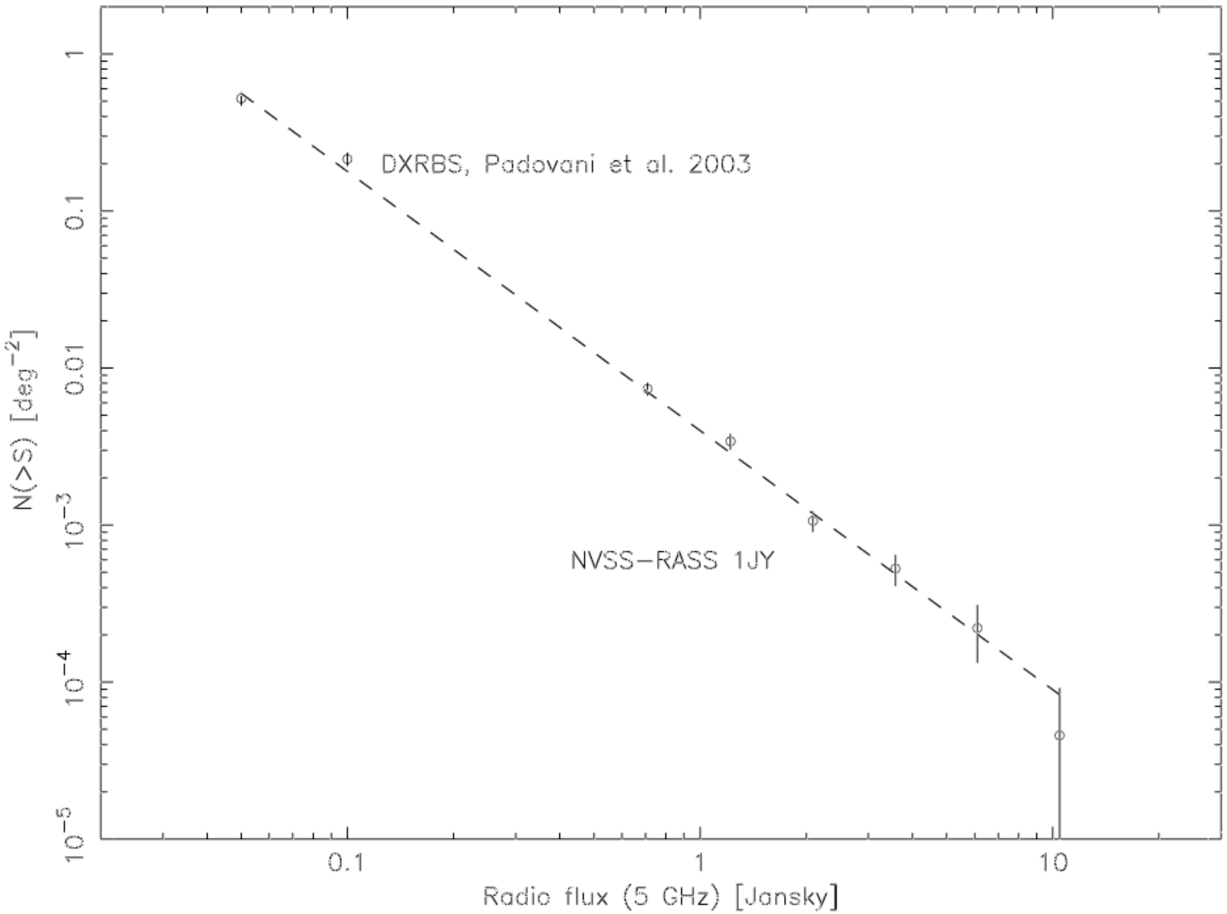

$$C_{\ell,Blazar} = \int_{S_{min}}^{S_{max}} dS \, \frac{dN}{dS} \, S^2$$

Giommi & Colafrancesco 2003

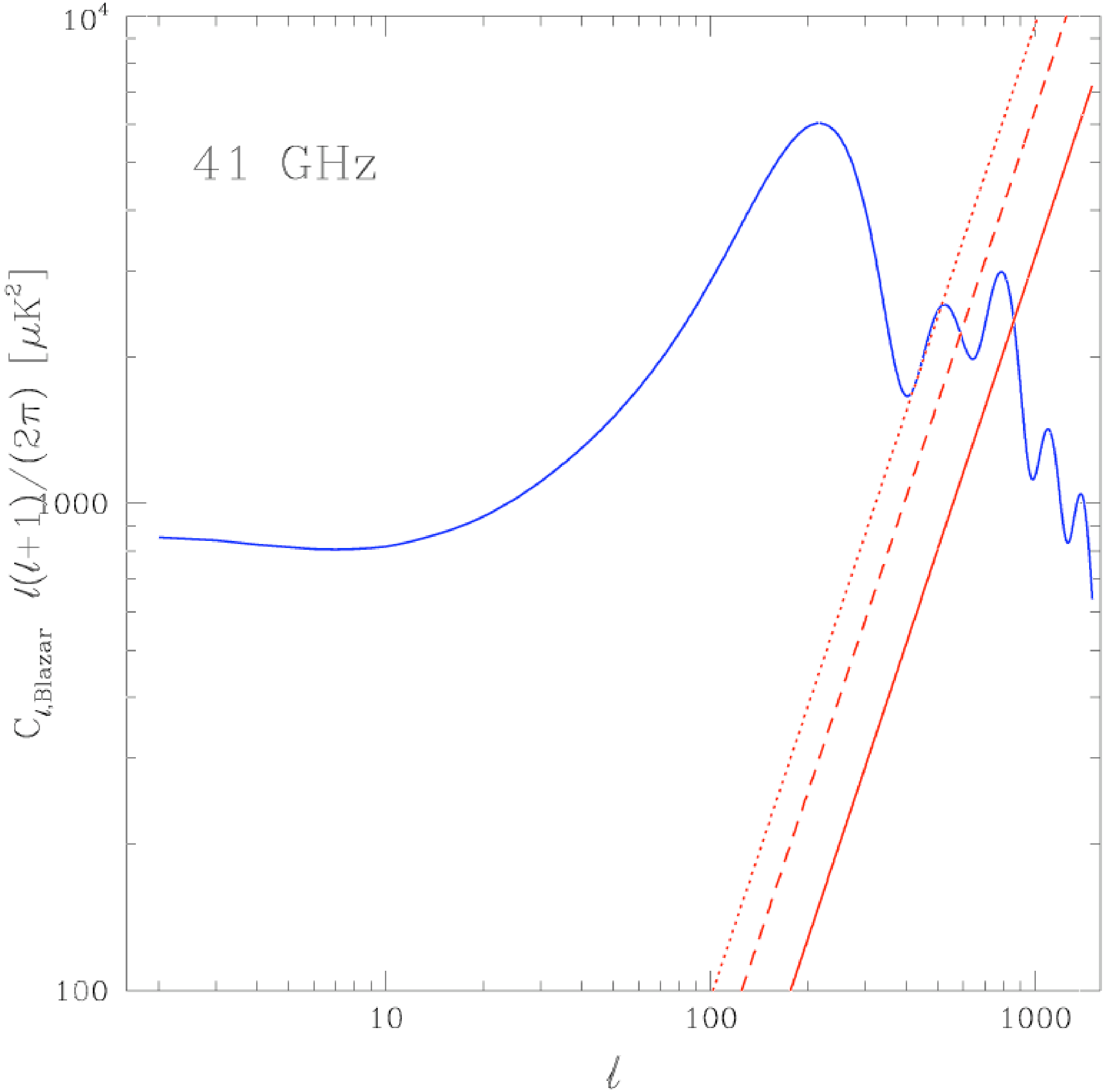

The Cosmic Energy Density Spectrum

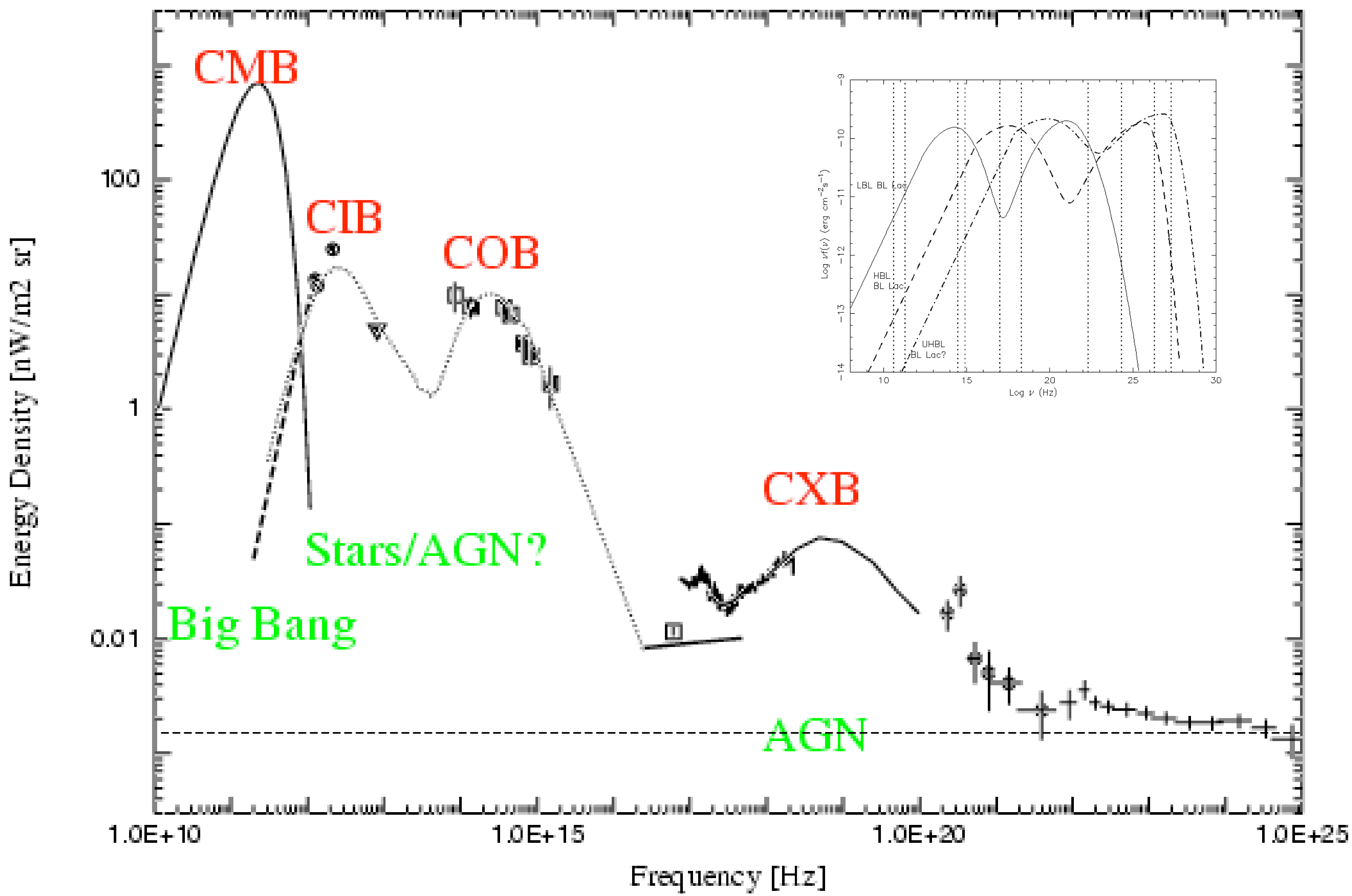

Swift detection of all previously undetected blazars in a micro-wave flux-limited sample of WMAP foreground sources

P. Giommi[1,2], M. Capalbi[1], E. Cavazzuti[1,2], S. Colafrancesco[3], A. Cucchiara[4], A. Falcone[4], J. Kennea[4],R. Nesci[5], M. Perri[1], G. Tagliaferri[6], A. Tramacere[5], G. Tosti[7], A. J. Blustin[8], G. Branduardi-Raymont[8], D. N. Burrows[4], G. Chincarini[6], A. J. Dean[9], N. Gehrels[10], H. Krimm[10], F. Marshall[10], A. M. Parsons[10], B. Zhang[11]

2007 *A&A*, 468, 571

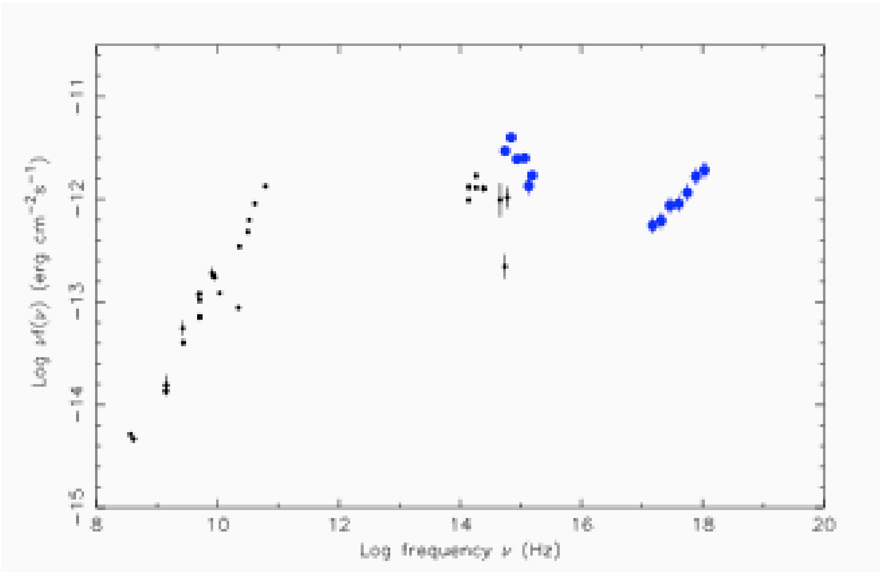

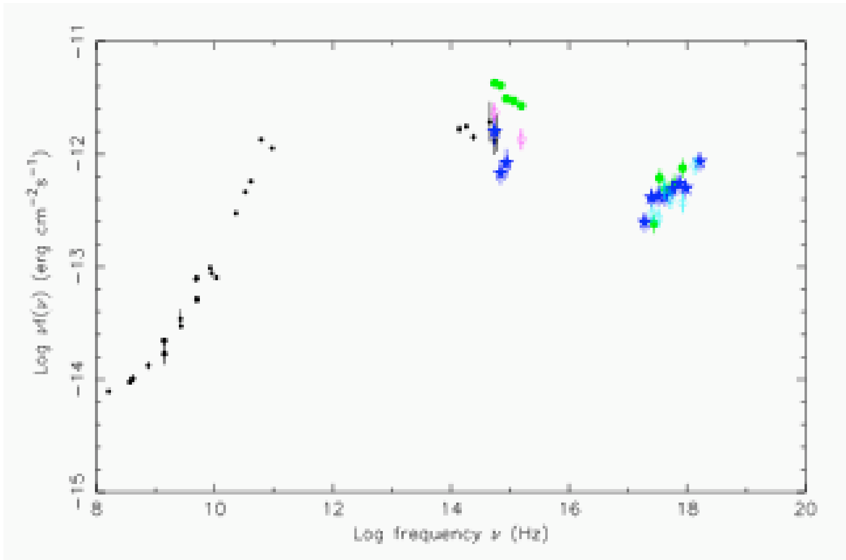

All microwave selected blazars are X-ray sources.

From μ–wave flux to X-rays and vice-versa

$$\alpha_{\mu x} = -\frac{\log(f_{94GHz}/f_{1keV})}{\log(\nu_{94GHz}/\nu_{1keV})} = -\frac{\log(f_{94GHz}/f_{1keV})}{6.41}$$

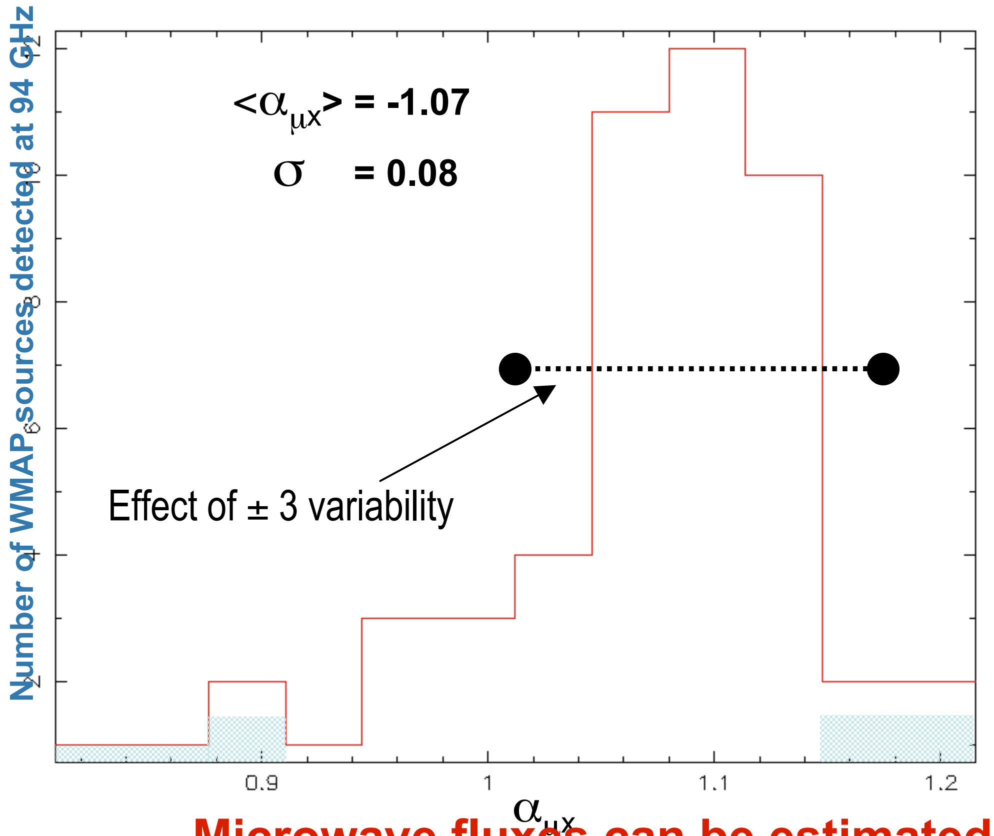

$$f_{94GHz} = f_{1keV} \cdot 10^{6.41 <\alpha_{\mu x}>}$$

$$f_{94GHz} = 10^{6.85} \cdot f_{1keV}$$

$$f_{94GHz} = 7.1 \cdot 10^{6}\, f_{1keV}$$

$$\sigma_{f_{94GHz}} = 10^{\,0.08 \cdot 6.41} \cdot f_{94GHz}$$

$$\sigma_{f_{94GHz}} \sim 3 \cdot f_{94GHz}$$

Microwave fluxes can be estimated from X-ray flux to within a factor ≤ 3

LBL Blazar contribution to soft CXB: 4%, total (LBL+HBL 12%)

From μ-wave to X-rays

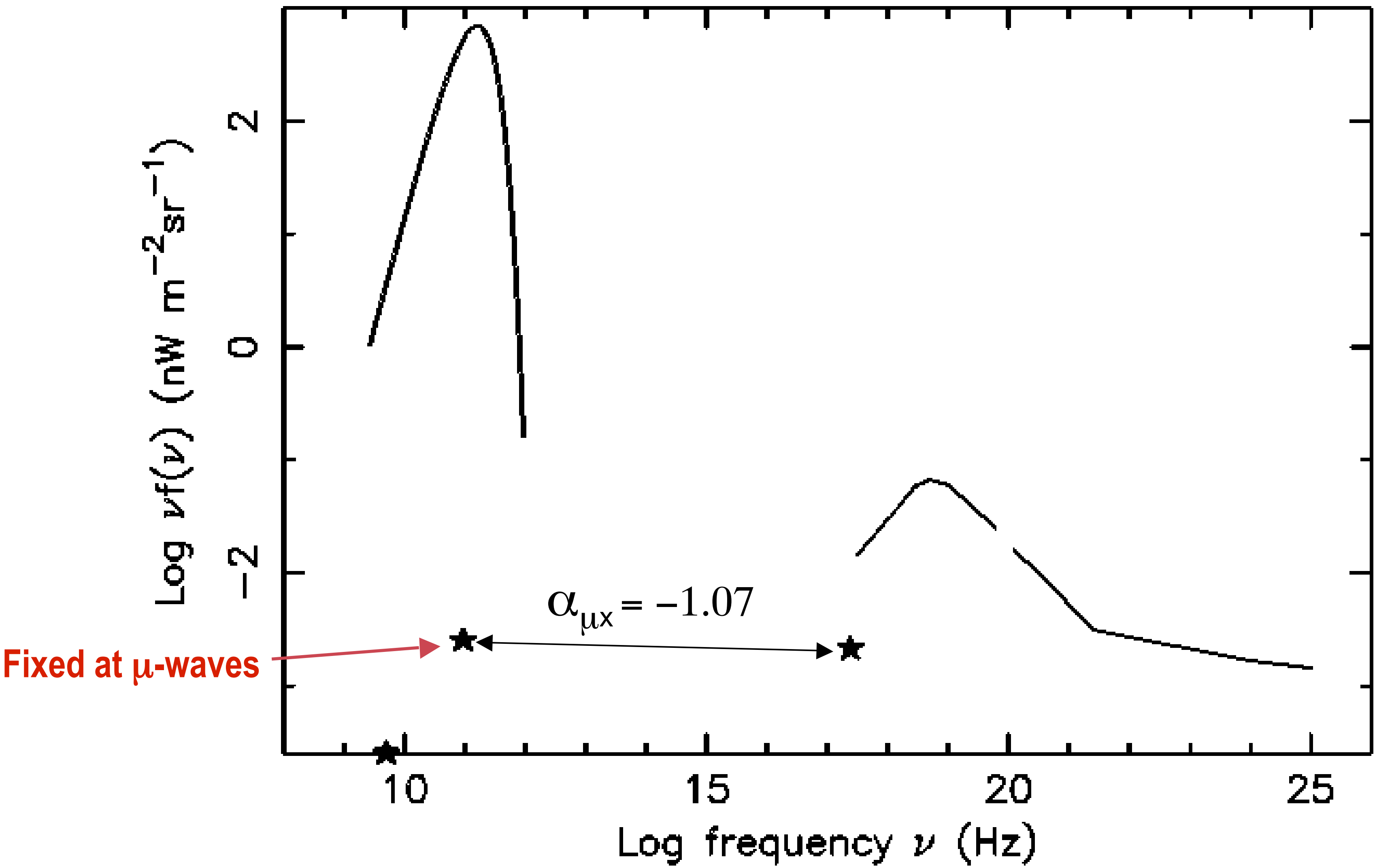

Hard-Xray/Soft Gamma-Ray Cosmic Background

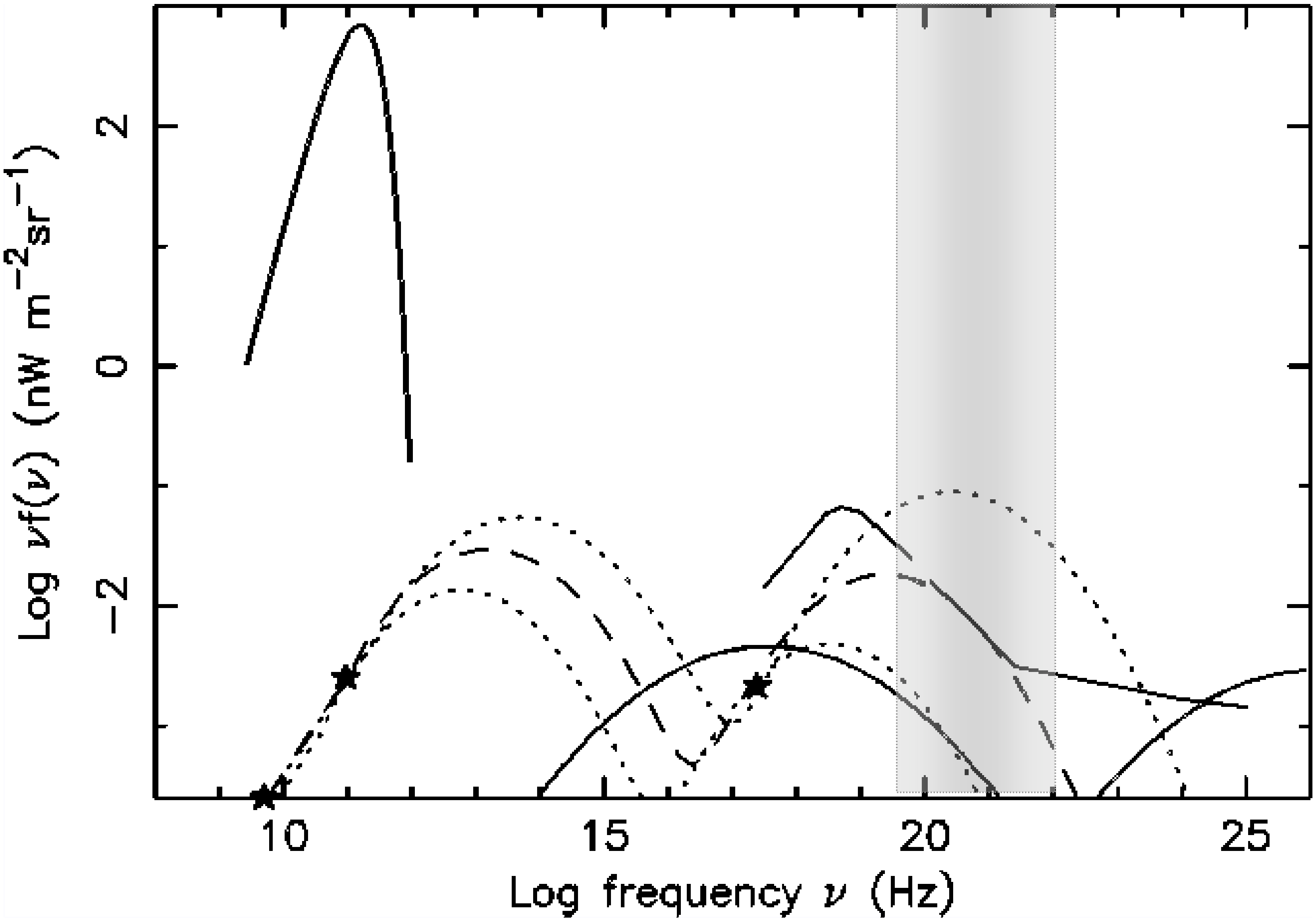

Contribution to the X and γ-ray backgrounds

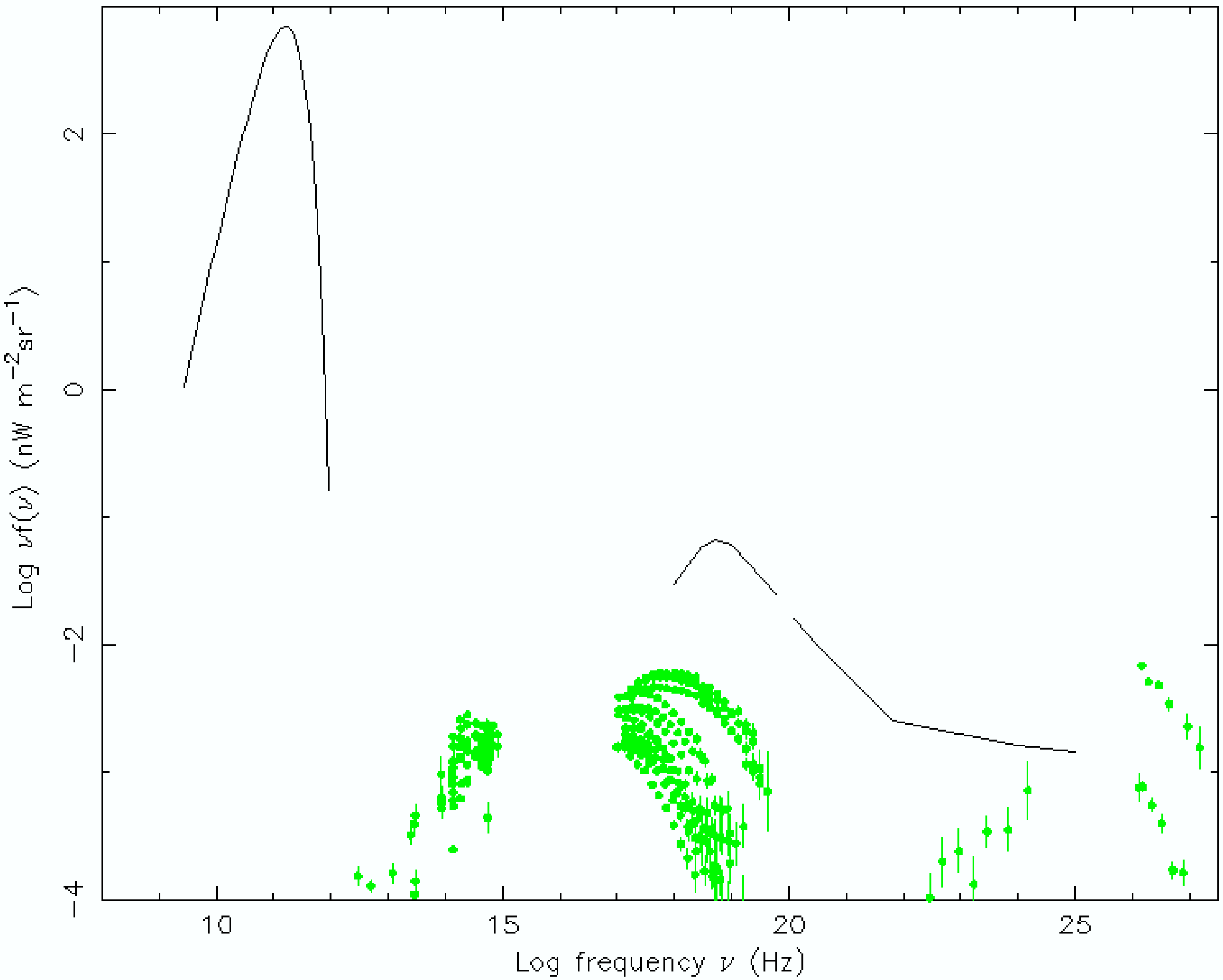

Radio — γ-ray flux ratio & duty cycle

Define a slope/trend: $$\alpha_{\mu\gamma} \equiv \frac{\log(F_\mu / F_\gamma)}{\log(\nu_\mu / \nu_\gamma)}$$

Blazar Name	$\alpha_{\mu\gamma}$	$f_{\gamma\text{-source}}/\langle\gamma\text{-background}\rangle$ ($\alpha_{\mu\gamma\,\mathrm{background}}$=-0.994)
BZQ J0204+1514	-0.892	14.5
BZU J0210-5101	-0.887	16.6
BZB J0339-0146	-0.902	11.2
BZQ J0423-0120	-0.907	9.7
BZQ J0455-4615	-0.913	8.3
BZQ J0457-2324	-0.908	9.6
BZU J0522-3627	-0.926	6.0
BZB J0538-4405	-0.892	14.4
BZQ J1256-0547 (3C 279)	-0.870	25.5

Duty cycle (%)
6.9
6.0
8.9
10.3
12.0
10.4
16.7
6.9
3.9

Table 2. The list and properties of all WMAP-detected Blazars associated to EGRET γ-ray sources

Blazar Name	R.A. J2000.0	Dec J2000.0	Radio Flux 5GHz Jy	WMAP flux 94GHz Jy	EGRET flux >100 MeV 10^{-8} ph cm^{-2} s^{-1}	$\alpha_{\mu\gamma}$	Duty cycle %	EGRET name 3EG J	WMAP catalog number
(1)	(2)	(3)	(4)	(5)	(6)	(7)	(8)	(9)	(10)
4C15.05	02 04 50.3	15 14 10	3.073	1.6^{*}	9-53	0.846-0.914	2-12	0204+1458	092
1Jy0208-512	02 10 46.2	−51 01 02	3.198	1.8	35-134	0.816-0.867	1-4	0210-5055	158
B2 0234+28	02 37 52.3	28 48 08	2.794	2.1^{*}	11-31	0.877-0.917	5-13	0239+2815	093
CTA26	03 39 30.8	−01 46 35	3.014	3.2	13-178	0.827-0.926	1-17	0340-0201	106
PKS 0420-01	04 23 15.7	−01 20 32	4.357	3.9	9.3-64.2	0.873-0.946	4-29	0422-0102	110
1Jy0454-463	04 55 50.7	−46 15 59	1.653	3.8	5.5-22.8	0.911-0.966	11-47	0458-4635	151
1Jy0454-234	04 57 03.1	−23 24 51	1.863	2.7	8.1-14.7	0.915-0.938	13-23	0456-2338	128
PKS 0506-61	05 06 44.0	−61 09 40	1.211	1.1^{*}	6-29	0.855-0.915	3-13	0512-6150	154
1Jy0537-441	05 38 51.3	−44 05 11	4.805	6.7	16.5-91.1	0.880-0.945	5-28	0540-4402	148
PKS 0735+178	07 38 07.3	17 42 18	1.812	1.7^{*}	15-29	0.872-0.896	4-8	0737+1721	113
B2 0827+24	08 30 52.0	24 10 57	0.886	2.6^{*}	16-111	0.837-0.911	2-11	0829+2413	112
S50836+710	08 41 24.4	70 53 40	2.342	1.2^{*}	9-33	0.854-0.903	2-9	0845+7049	089
OJ 287	08 54 48.8	20 06 30	2.908	2.5	9.7-15.8	0.910-0.928	11-18	0853+1941	115
4C 29.45	11 59 31.7	29 14 43	1.461	2.1	7.5-163.2	0.814-0.931	1-19	1200+2847	111
PKS1221-82[a]	12 24 54.3	−83 13 10	0.797	1.2^{*}	11-36	0.850-0.895	2-7	1249-8330	178
1Jy1226+023	12 29 06.3	02 03 04	36.923	9.0	8.5-48.3	0.916-0.982	13-73	1229+0210	170
3C279	12 56 11.0	−05 47 19	11.192	19.0	15-250	0.882-1.000	5-100	1255-0549	181
PKS 1313-333	13 16 07.9	−33 38 59	1.093	1.3^{*}	15-32	0.858-0.887	3-6	1314-3431	182
1Jy1406-076	14 08 56.4	−07 52 25	1.080	1.7^{*}	10-128	0.815-0.912	1-12	1409-0745	203
1Jy1424-418	14 27 56.2	−42 06 19	2.597	1.5^{*}	12-55	0.842-0.901	2-9	1429-4217	191
1Jy1510-089	15 12 50.4	−09 06 00	3.080	1.7	12.6-49.4	0.851-0.903	2-9	1512-0849	207
1Jy1606+106	16 08 46.0	10 29 07	1.412	3.1	21.0-62.4	0.865-0.907	3-10	1608+1055	009
DA 406	16 13 40.9	34 12 46	2.324	1.4	19-68.9	0.831-0.880	1-5	1614+3424	023
4C38.41	16 35 15.4	38 08 04	3.221	4.2	31.8-107.5	0.856-0.902	3-9	1635+3813	033
PMNJ1703-6212	17 03 36.2	−62 12 39	0.616	1.9^{*}	14-53	0.853-0.904	2-9	1659-6251[b]	198
S41739+522	17 40 36.9	52 11 42	1.699	1.2^{*}	10-45	0.842-0.899	2-8	1738+5203	048
PKS 1814-63[c]	18 19 34.9	−63 45 47	4.506	1.3^{*}	14-27	0.864-0.889	3-6	1813-6419	200
PMNJ1923-2104	19 23 32.1	−21 04 33	2.885	2.1^{*}	29^{**}	0.880	5	1921-2015	008
PKS 2052-47	20 56 15.5	−47 14 37	2.026	1.3^{*}	9-35	0.854-0.906	3-10	2055-4716	208
BL Lac	22 02 43.2	42 16 39	2.940	3.8^{*}	9-40	0.890-0.947	7-29	2202+4217	058
PKS2209+236	22 12 05.9	23 55 39	1.123	1.3^{*}	7-46	0.844-0.916	2-13	2209+2401	050
CTA102	22 32 36.3	11 43 50	3.967	3.1	12.1-51.6	0.873-0.928	4-18	2232+1147	047
1Jy2251+158	22 53 57.6	16 08 52	14.468	5.9	24.6-116.1	0.866-0.925	3-16	2254+1601	055
1Jy2351+456	23 54 21.6	45 53 03	1.127	1.7^{*}	12-43	0.874-0.923	4-15	2358+4604	074

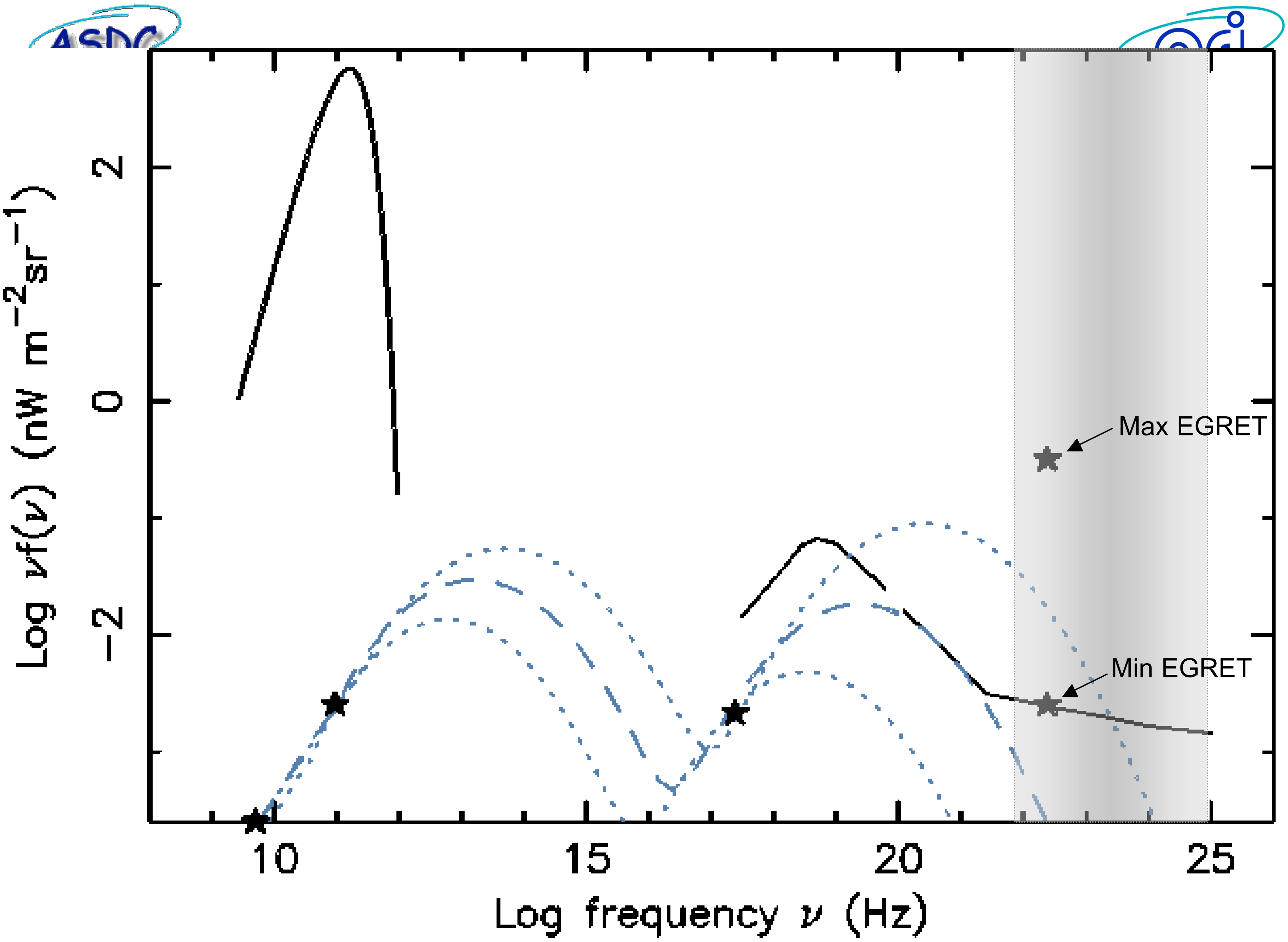

Log νf(ν) (nW m^{-2}sr^{-1})
Log frequency ν (Hz)
Max EGRET
Min EGRET
2
0
−2
10
15
20
25

A ~10 mJy Blazar